Li, G., Wang, X., Yang, H., Jin, M., Qin, C., Wang, Y., Jonell, T.N., Pan, L., Chen, C., Zhao, W., Zhang, X., and Madsen, D.B., 2024, Asynchronous Holocene lake evolution in arid mid-latitude Asia is driven by glacial meltwater and variations in Westerlies and the East Asian summer monsoon: GSA Bulletin, https://doi.org/10.1130/ B37288.1

Supplemental Material

Supplemental Text S1. Luminescence dating: sample preparation and analytical facilities.

Supplemental Text S2. Quartz OSL dating, single aliquot and single grain K-feldspar pIRIR dating measurement, and dose rate determination

Figure S1. The photograph of paleolake shorelines sections from Aibi Lake Basin.

Figure S2. Luminescence characteristics of quartz samples from the Aibi Lake Basin: (a) decay curve for quartz sample AB18-3-45; and (b), (c), (d) OSL IR depletion ratios, the recycling ratios, and the recuperation of the natural signals for all 35 quartz samples from the Aibi Lake Basin.

Figure S3. Plots of ranked individual D_e distributions (top row) against to their intrinsic brightness increasing for five well-bleached shoreline samples. The plot of CAM D_e values (middle row), and OD values (bottom row) distributions for the grains with brightness above different N-L1 thresholds. The blue line is the N-L1 threshold for 30% brightest grains for each sample.

Figure S4. Abanico plots (left) and Kernel Density Estimates (KDEs; right) of all single-grain samples from the shorelines in the Aibi Lake Basin.

Figure S5. The reconstructed lake covering area changes of Aibi Lake during past 18 ka.

Table S1. Information for samples collected from paleoshorelines in the Aibi Lake Basin.

Table S2. Protocol for quartz OSL dating and K-feldspar single-aliquot and single-grain pIRIR dating used for the De measurements of shoreline samples.

Table S3. Summary of the residual doses for the IR_{50} and $pIR_{50}IR_{170}$ signals after 28h bleaching under sunlight for the single-aliquot K-feldspar samples from the Aibi Lake Basin shorelines.

Table S4. Summary of the single-aliquot pIRIR ages and the single-grain pIRIR CAM ages for the K-feldspar samples from paleoshorelines in the Aibi Lake Basin.

Table S5. Summary of accepted grains passing the rejection criteria for K-feldspar samples from the Aibi Lake Basin.

Table S6. Summary of single-grain pIRIR dating results for samples from the Aibi Lake Basin.

Supplemental Text S1: Luminescence dating: sample preparation and analytical facilities

A total of 59 luminescence dating samples were prepared in a darkroom under weak red light. Standard heavy liquid separation employing liquids with densities of 2.58 g/cm^3, 2.62 g/cm^3, and 2.75 g/cm^3 was used to retrieve and concentrate coarse-grained (>63 μm) quartz and K-feldspar fractions. Quartz fractions were etched using 40 % HF for at least 90 minutes to remove the alpha irradiation layers and any remaining feldspar grains or adhering feldspar. The K-feldspar fractions were etched using 10 % HF for 40 minutes to remove the alpha irradiation layers. Of all 59 samples, 24 samples did not yield quartz fractions, and only nineteen 150–250 μm and sixteen 63–150 μm quartz fractions were retrieved. However, only three pure quartz samples within the 63–90 μm and 90–125 μm fractions were retrieved after purity checks using OSL IR depletion ratio tests (Duller, 2003). A total of ten 63-90 μm, two 90-125μm, one 125-150 μm, six 150-180 μm and forty 180–250 μm K-feldspar samples were retrieved for age determination.

All luminescence measurements were performed on two Risø TL/OSL-DA-20 reader luminescence dating systems (Bøtter-Jensen et al., 2010) at Lanzhou University. A $^{90}Sr/^{90}Y$ beta source was used for laboratory irradiation and was calibrated for both disc and cup geometry. Quartz OSL signals were stimulated using blue LEDs (470 nm, ~80 mW/cm^2) and detected using a 7.5 mm of Schott U-340 (UV) glass filter. K-feldspar single-aliquot IR and pIRIR signals were stimulated using IR LEDs (870 nm, ~135 mW/cm^2), and detected through a Schott BG 39/Corning 7-59 filter combination. Single-grain IR and pIRIR signals were stimulated using IR laser and detected using a BG 39 filter without quartz windows.

Supplemental Text S2: Quartz OSL dating, single aliquot and single grain K-feldspar pIRIR dating measurement, and dose rate determination

A standard single-aliquot regeneration (SAR) protocol was used for the three quartz samples for luminescence characteristics measurements (Murray and Wintle, 2003). A 7–8 mm aliquot size with thousands of grains was used to retrieve a detectable quartz OSL signal. The quartz OSL signal was derived from the first 0.32 s integral of the decay curve minus the early background (0.32–0.96 s) to minimize the influence of interfering medium and slow components (Cunningham & Wallinga, 2010). OSL IR depletion ratio tests were conducted on all 35 quartz samples to check for purity (Duller, 2003).

In order to validate the thermal treatments in the pIRIR dating protocol for the shoreline samples, prior-IR stimulation temperature to D_e plateau tests were performed on the coarse K-feldspar fraction (180–250 µm) of sample AB18-7-235 using a 2 mm aliquot. Preheat temperatures from 160 to 240 °C with 20 °C intervals were used for six groups of aliquots (three aliquots in each group, 18 aliquots in total). The pIRIR stimulation was always 30 °C lower than the corresponding preheat temperature. A pIRIR dating protocol using a preheat temperature of 320 °C and a pIRIR stimulation of 290 °C was also tested (i.e., Thiel et al, 2011). An IRSL hot stimulation using a temperature 5 °C higher than the preheat temperature was conducted at the end of each cycle.

In order to check the stability of the $pIRIR_{170}$ signal, an anomalous fading test (fading rate or g value measurements; Aitken, 1985; Auclair et al., 2003) was conducted on coarse-grained K-feldspar sample AB18-6-195. The same dose was given repeatedly with different delay periods (e.g. 0, 0.5, 1, 2, 4, 22, and 175 h) between the end of preheat and the start of the IRSL measurement. The decay in the sensitivity-corrected $pIRIR_{170}$ signals as a function of storage time at room temperature was measured. The calculated g values were normalized to a measurement time of 2 days after irradiation (Huntley and Lamothe, 2001).

Dose recovery tests were conducted on sunlight bleached samples AB18-1-160 (28 h sunlight bleaching, Nov, 2018, Lanzhou, China) and JH19-4-180 (28 h sunlight bleaching, Nov, 2019, Lanzhou, China) to check the suitability of the single-aliquot pIRIR dating protocol. This protocol utilized a $pIR_{50}IR_{170}$ signal stimulated at 170ºC following an IR stimulation at 50 ºC for single-aliquots of the 180–250 µm fractions. Given doses of 122 Gy and 62.8 Gy were added to the sunlight-bleached 180–250 µm K-feldspar samples AB18-1-160 and JH19-4-180, respectively, and were measured as an unknown dose using the protocol in Table S2. In the single-aliquot pIRIR dating protocol, a test dose of at least 30% of the D_es was used for sensitivity corrections (Yi et al., 2016). IRSL and pIRIR signals were derived from the integral of the initial 2 s of the decay curves minus the last 49 s background integral. Sunlight bleach tests were conducted on K-feldspar (180–250 µm fractions) for 28 h (4 h each day, 7 days, Nov, 2019, Lanzhou, China) after which the residual doses were measured using the pIRIR dating protocol (Table S3).

For single-grain pIRIR dating, the IR and pIRIR signals were measured on single-grain discs with 300 µm hole diameters using the pIRIR dating protocol (Table S2). Single-grain discs of each K-feldspar sample were randomly checked for the number of grains in each hole under microscope. More than a single-grain per disc hole was rarely observed. IR and pIRIR signals used for D_e determination were derived by subtracting a background estimated from the last 0.33 s from the first 0.15 s of the decay curve for single-grains.

Dose recovery tests were carried out on 180–250 µm K-feldspar samples AB18-1-65 and JH19-2-120 to check the suitability of the single-grain pIRIR dating protocol. For each sample, four single-grain aliquots were bleached under sunlight for 28 h. Residual doses for the pIRIR signals of two aliquots for each K-feldspar sample were measured using the single-grain pIRIR dating protocol (Table S2). Dose recovery tests were conducted on the other two bleached aliquots of the single-grain K-feldspar samples using the same dating protocol. Laboratory given doses of 68.82 Gy and 50.68 Gy were added to sample AB18-1-65 and JH19-2-120, respectively. The test dose of 50% of given dose were used for the dose recovery test. The measured residual doses were subtracted from measured pIRIR single-grain D_es in the measured/given dose ratio calculations.

External dose rates for quartz and K-feldspar samples were determined by powdering 3–5 g of each sample in preparation for determination of U and Th concentrations by ICP-MS and K content by ICP-OES at Lanzhou University. These concentrations were used to calculated gamma and beta dose rates using the conversion factor of Guérin et al. (2011). Internal dose rates were determined by analyzing the individual K content of 84 K-feldspar grains from eight samples across different shoreline sections by electron microprobe analysis (EMPA). Analytical discs were prepared by affixing individual K-feldspar grains using liquid, quick-hardening resin to the discs. Once dried, discs were then ground to expose grain cross-sections, polished and carbon-coated immediately prior to EMPA to avoid charging during measurement.

The cosmic dose rates of the quartz and K-feldspar samples were calculated using sample altitudes and burial depths (Prescott and Hutton, 1994). The measured water content of shoreline samples is <5 %, while the saturation moisture content of most paleoshoreline samples varied between 10 % and 30 %. The life-time water content of each sample was estimated according to the measured water content and saturation water content changes for shorelines samples due to lake level duration and fluctuation at different locations. The D_e values and dose rate of quartz and K-feldspar samples were calculated using the LDAC program v1.0 (Liang and Forman, 2019).

References

Aitken, M.J., 1985. Thermoluminescence Dating: London, Academic Press.

Auclair, M., Lamothe, M., Huot, S., 2003, Measurement of anomalous fading for feldspar IRSL using SAR: Radiation Measurements, v. 37, p. 487–492.

Bøtter-Jensen, L., Thomsen, K.J, Jain, M., 2010, Review of optically stimulated luminescence (OSL) instrumental developments for retrospective dosimetry: Radiation Measurements, v. 45, p. 253–257.

Cunningham, A.C., Wallinga, J., 2010, Selection of integration time intervals for quartz OSL decay curves: Quaternary Geochronology, v. 5, p. 657–666.

Duller, G.A.T., 2003, Distinguishing quartz and feldspar in single grain luminescence measurements: Radiation Measurements, v. 37, p. 161–165.

Guérin, G., Mercier, N., Adamiec, G., 2011, Dose-rate conversion factors: update: Ancient TL, v. 29, p. 5–8.

Huntley, D.J., Lamothe, M., 2001, Ubiquity of anomalous fading in K-feldspars and the measurement and correction for it in optical dating: Canadian Journal of Earth Sciences, v. 38, p. 1093–1106.

Liang, P., Forman, S.L., 2019, LDAC: an Excel-based program for luminescence equivalent dose and burial age calculations: Ancient TL, v. 37, p. 21–40.

Murray, A.S., Wintle, A.G., 2003, The single aliquot regenerative dose protocol: potential for improvements in reliability: Radiation Measurements, v. 37, p. 377–381.

Prescott, J.R., Hutton, J.T., 1994, Cosmic ray contributions to dose rates for luminescence and ESR dating: large depths and long-term time variations: Radiation Measurements, v. 23, p. 497–500.

Thiel, C., Buylaert, J.P., Murray, A.S., Terhorst, B., Hofer, I., Tsukamoto, S., Frechen, M., 2011, Luminescence dating of the Stratzing loess profile (Austria) - Testing the potential of an elevated temperature post-IR IRSL protocol: Quaternary International, v. 234, p. 23–31.

Yi, S., Buylaert, J. P., Murray, A. S., Lu, H., Thiel, C., Zeng, L. 2016, A detailed post-IR IRSL dating study of the Niuyangzigou loess site in northeastern China: Boreas, v. 45, p. 644–657.

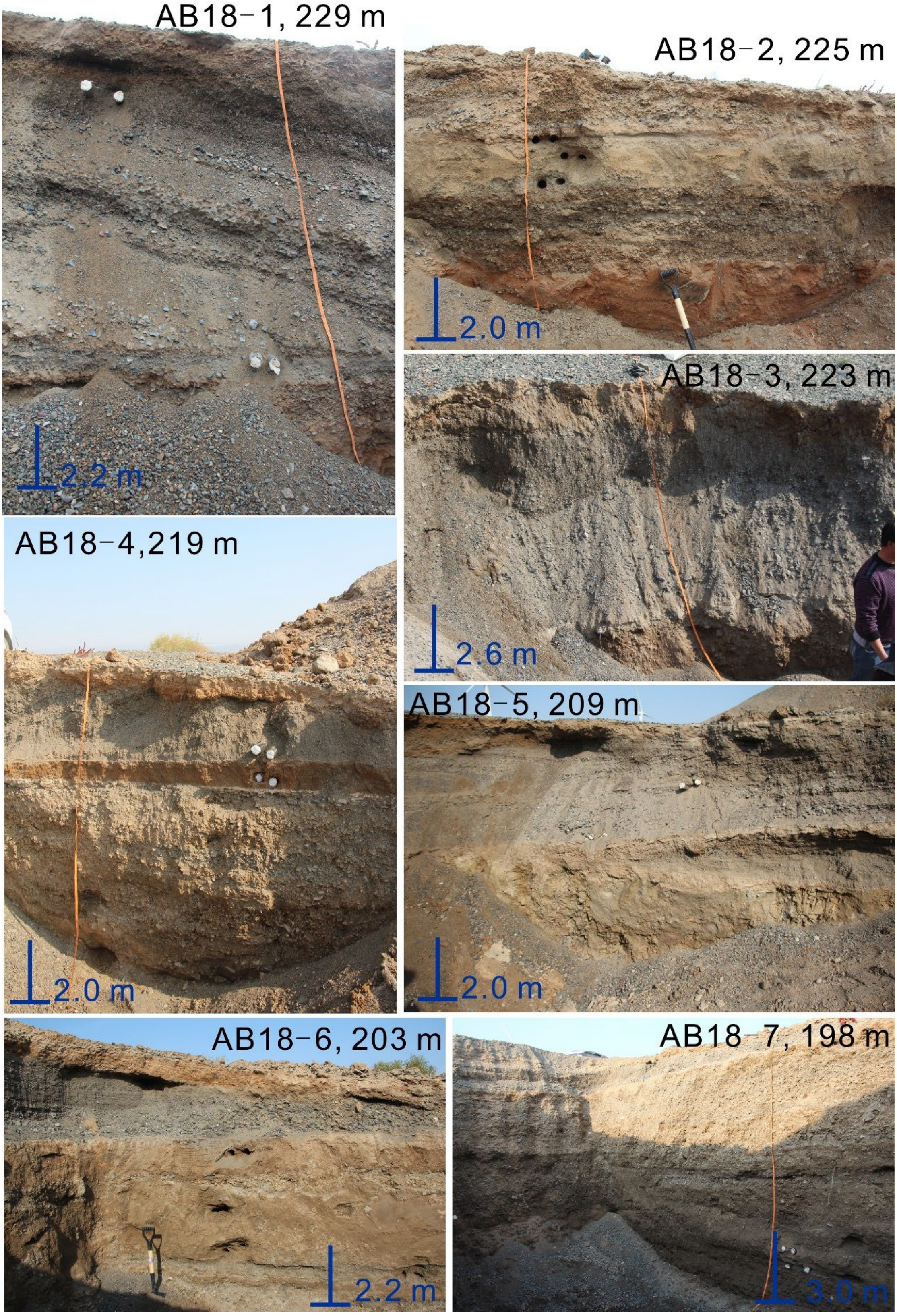
AB18-1, 229 m
2.2 m
AB18-2, 225 m
2.0 m
AB18-3, 223 m
2.6 m
AB18-4,219 m
2.0 m
AB18-5, 209 m
2.0 m
AB18-6, 203 m
2.2 m
AB18-7, 198 m
3.0 m

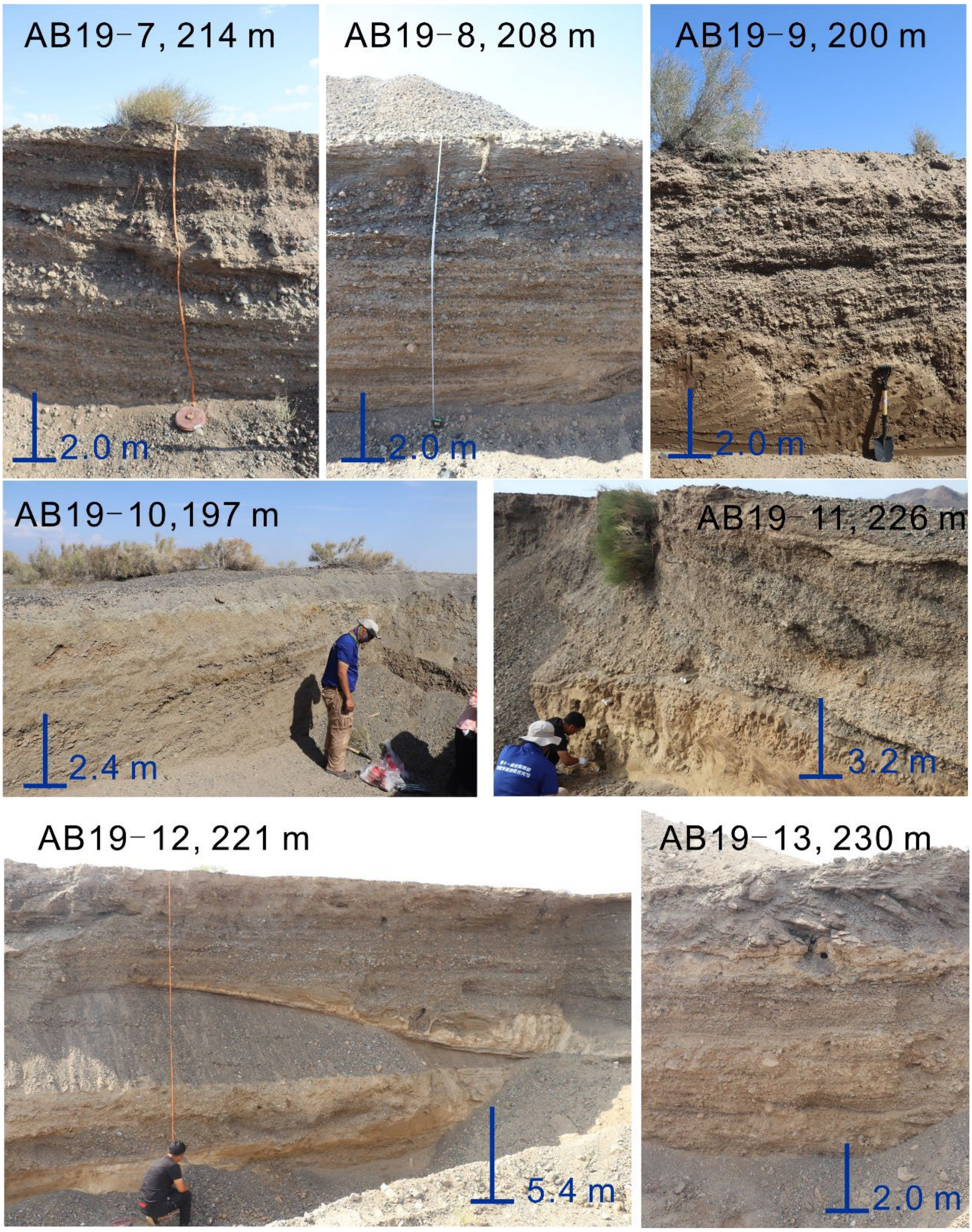
AB19-7, 214 m
2.0 m
AB19-8, 208 m
2.0 m
AB19-9, 200 m
2.0 m
AB19-10,197 m
2.4 m
AB19-11, 226 m
3.2 m
AB19-12, 221 m
5.4 m
AB19-13, 230 m
2.0 m

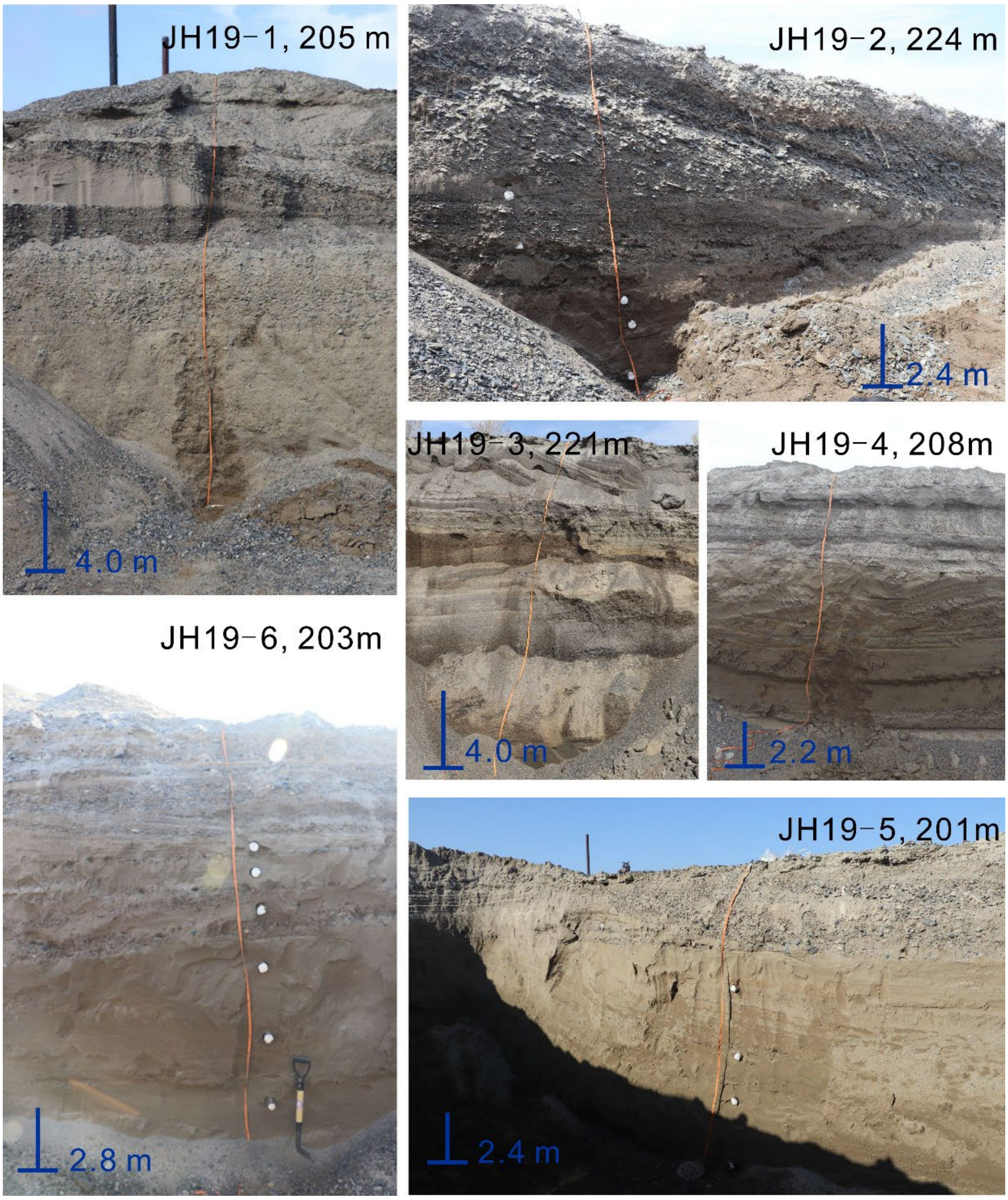

Figure S1. The photograph of paleolake shorelines sections from Aibi Lake Basin.

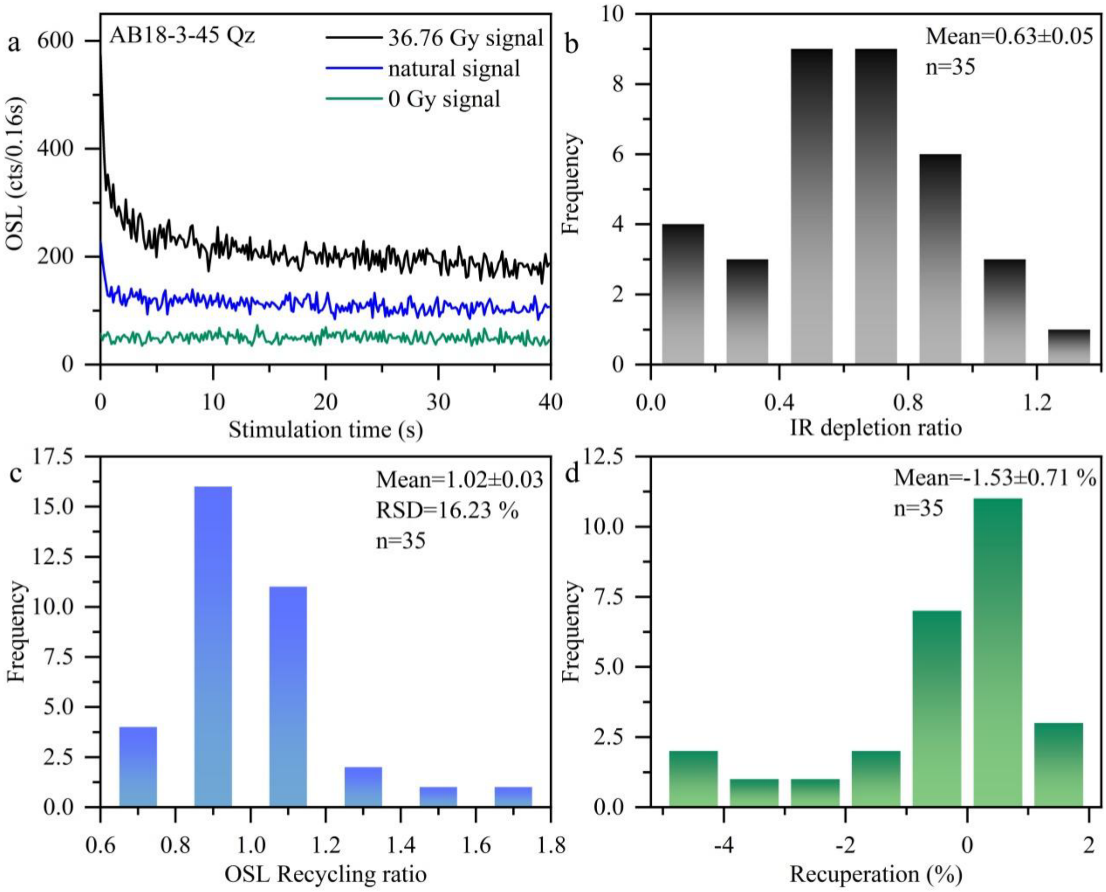

Figure S2. Luminescence characteristics of quartz samples from the Aibi Lake Basin: (a) decay curve for quartz sample AB18-3-45; and (b), (c), (d) OSL IR depletion ratios, the recycling ratios, and the recuperation of the natural signals for all 35 quartz samples from the Aibi Lake Basin.

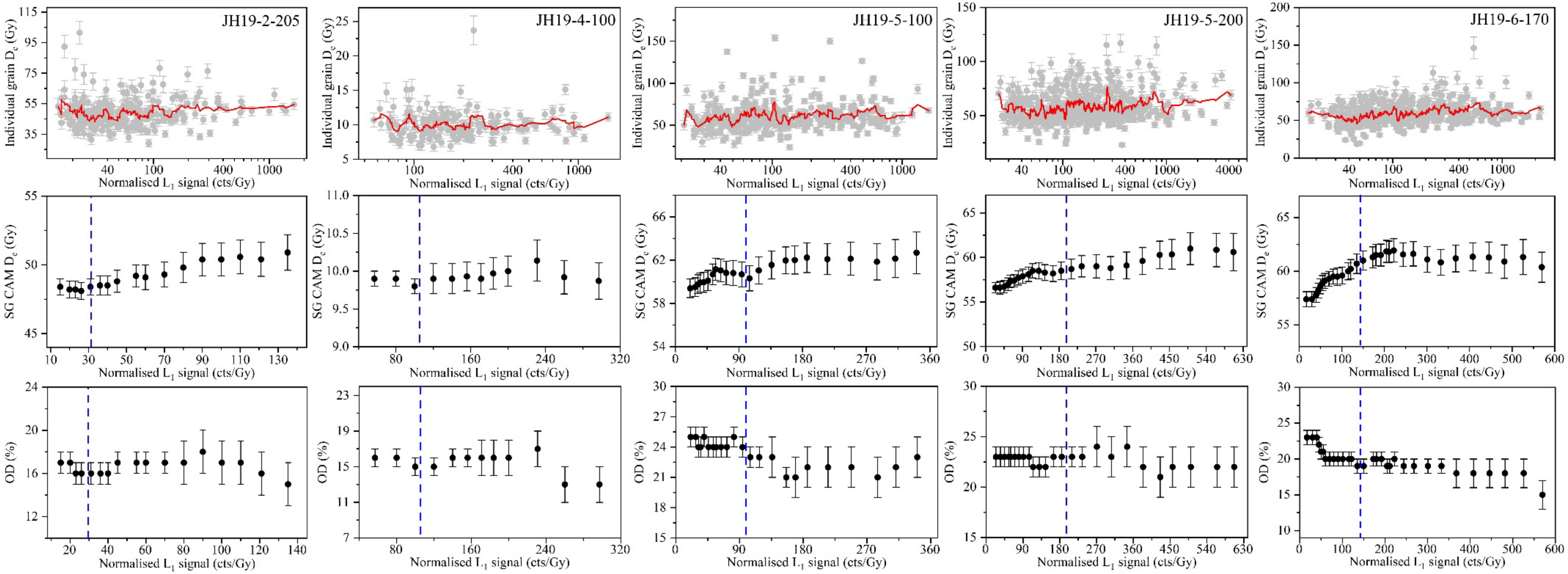

Figure S3. Plots of ranked individual D_e distributions (top row) against to their intrinsic brightness increasing for five well-bleached shoreline samples. The plot of CAM D_e values (middle row), and OD values (bottom row) distributions for the grains with brightness above different N-L1 thresholds. The blue line is the N-L1 threshold for 30% brightest grains for each sample.

Eolian Sediments (5)

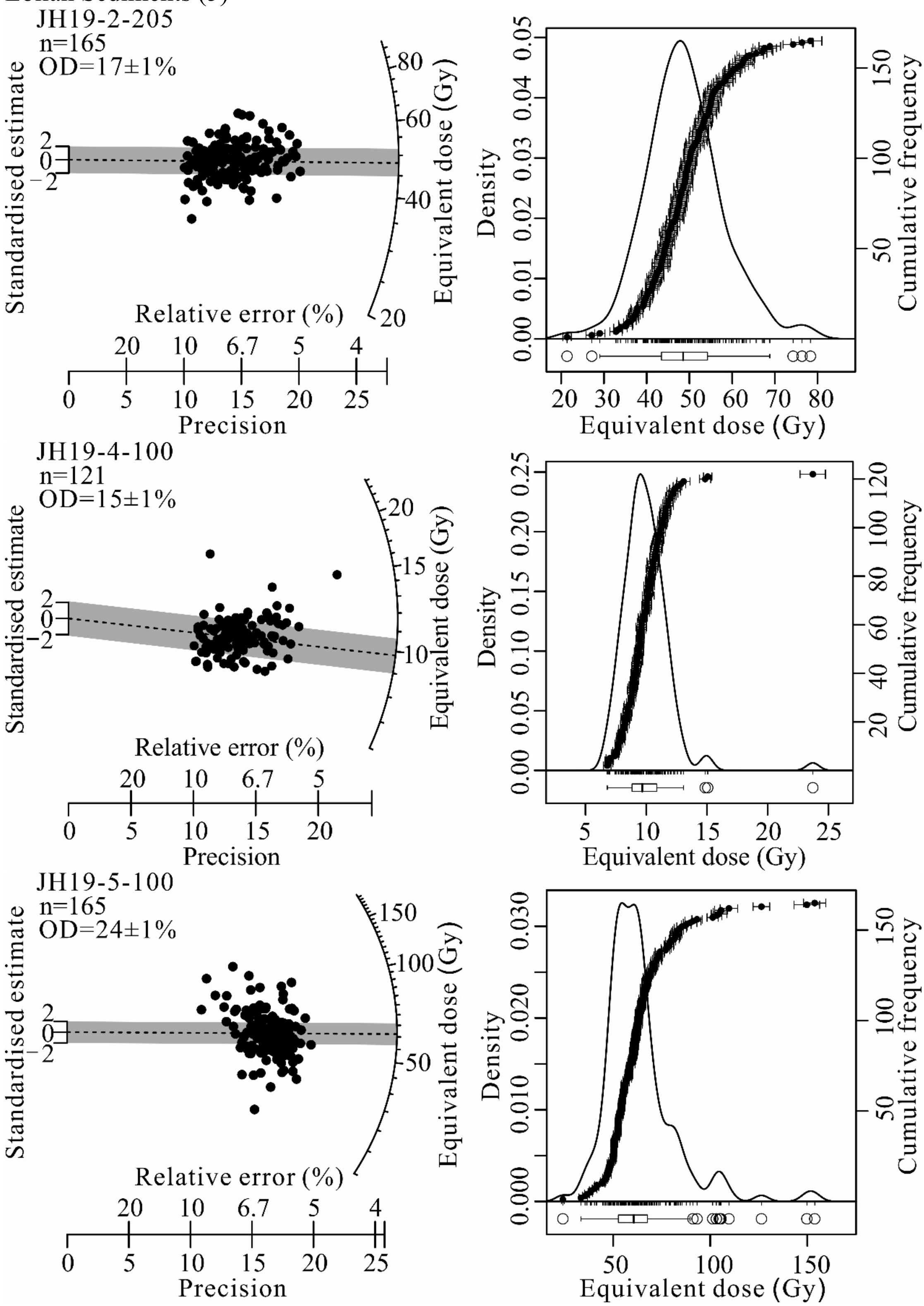

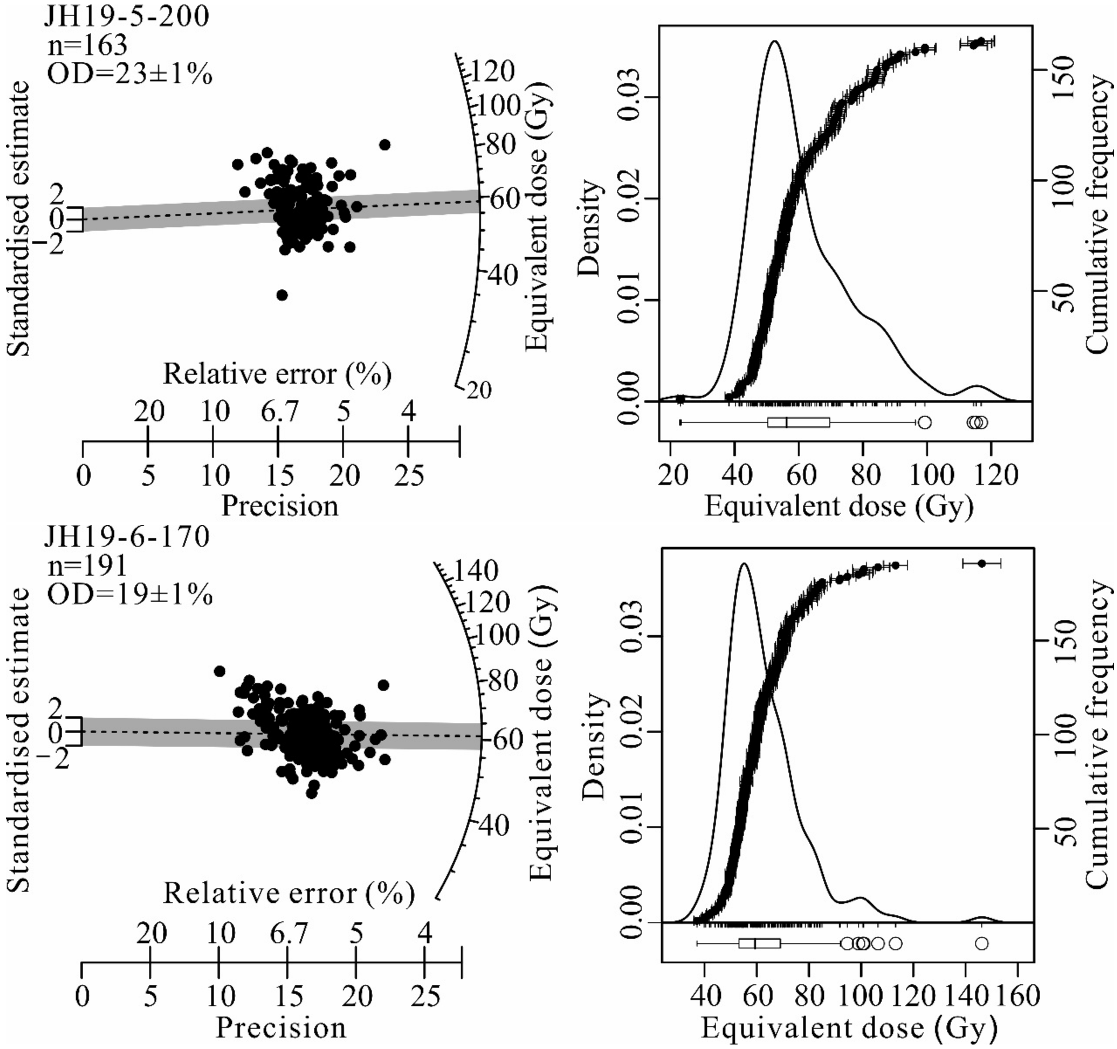

JH19-5-200
n=163
OD=23±1%
Standardised estimate
Relative error (%)
Precision
Equivalent dose (Gy)
Density
Cumulative frequency
JH19-6-170
n=191
OD=19±1%

Lake Sediments (39)

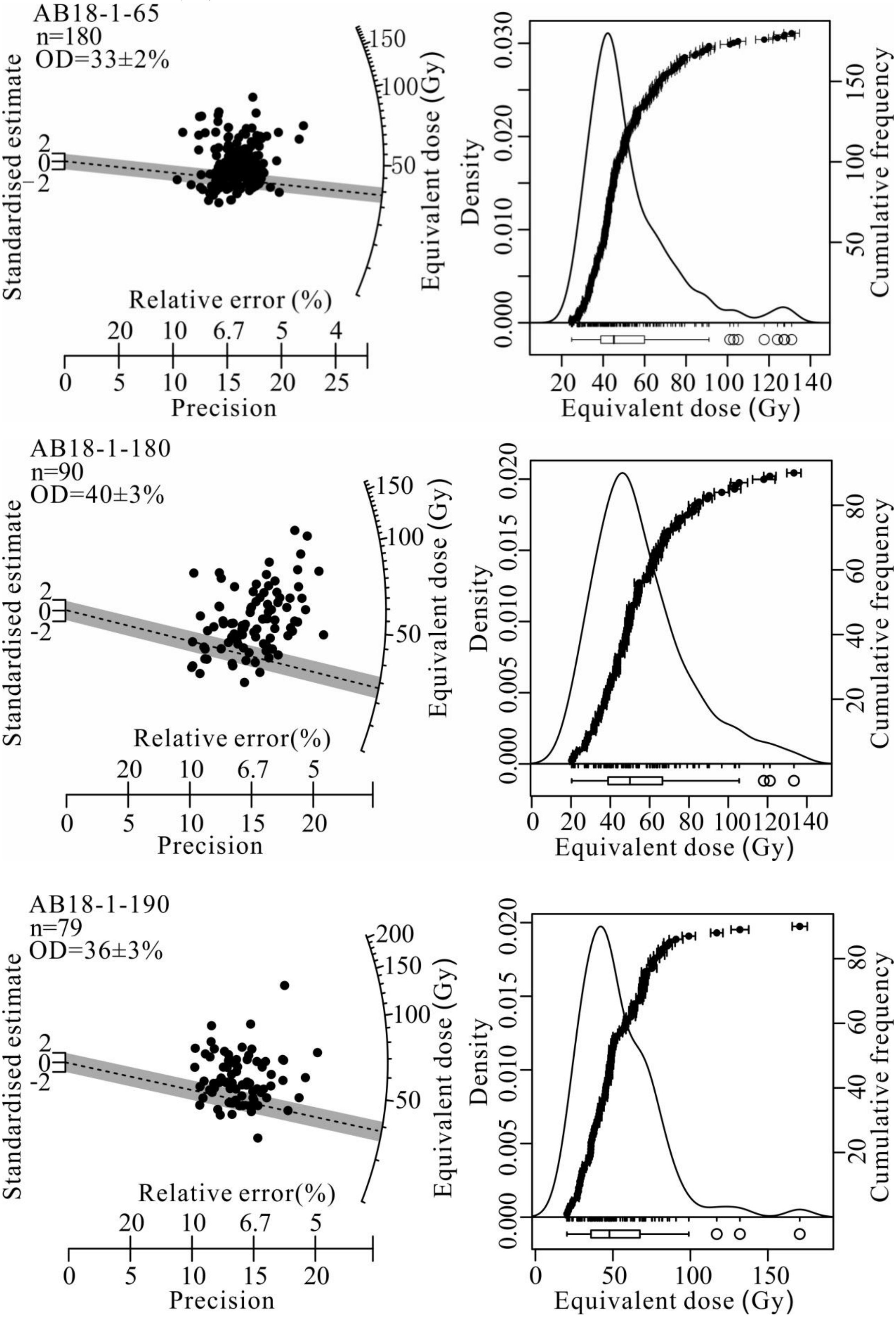

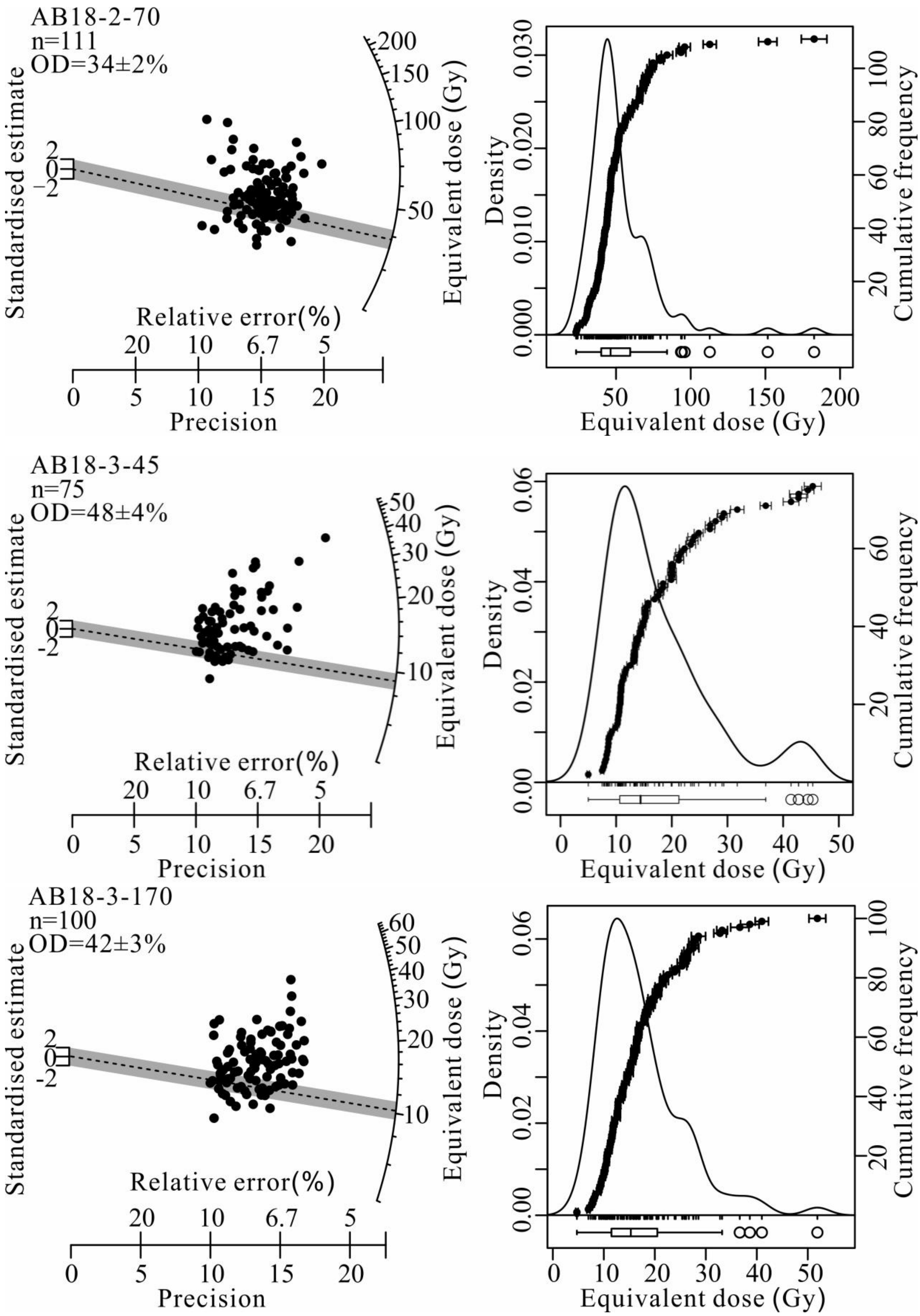
AB18-2-70
n=111
OD=34±2%
Standardised estimate
Relative error(%)
Precision
Equivalent dose (Gy)
Density
Cumulative frequency
AB18-3-45
n=75
OD=48±4%
AB18-3-170
n=100
OD=42±3%

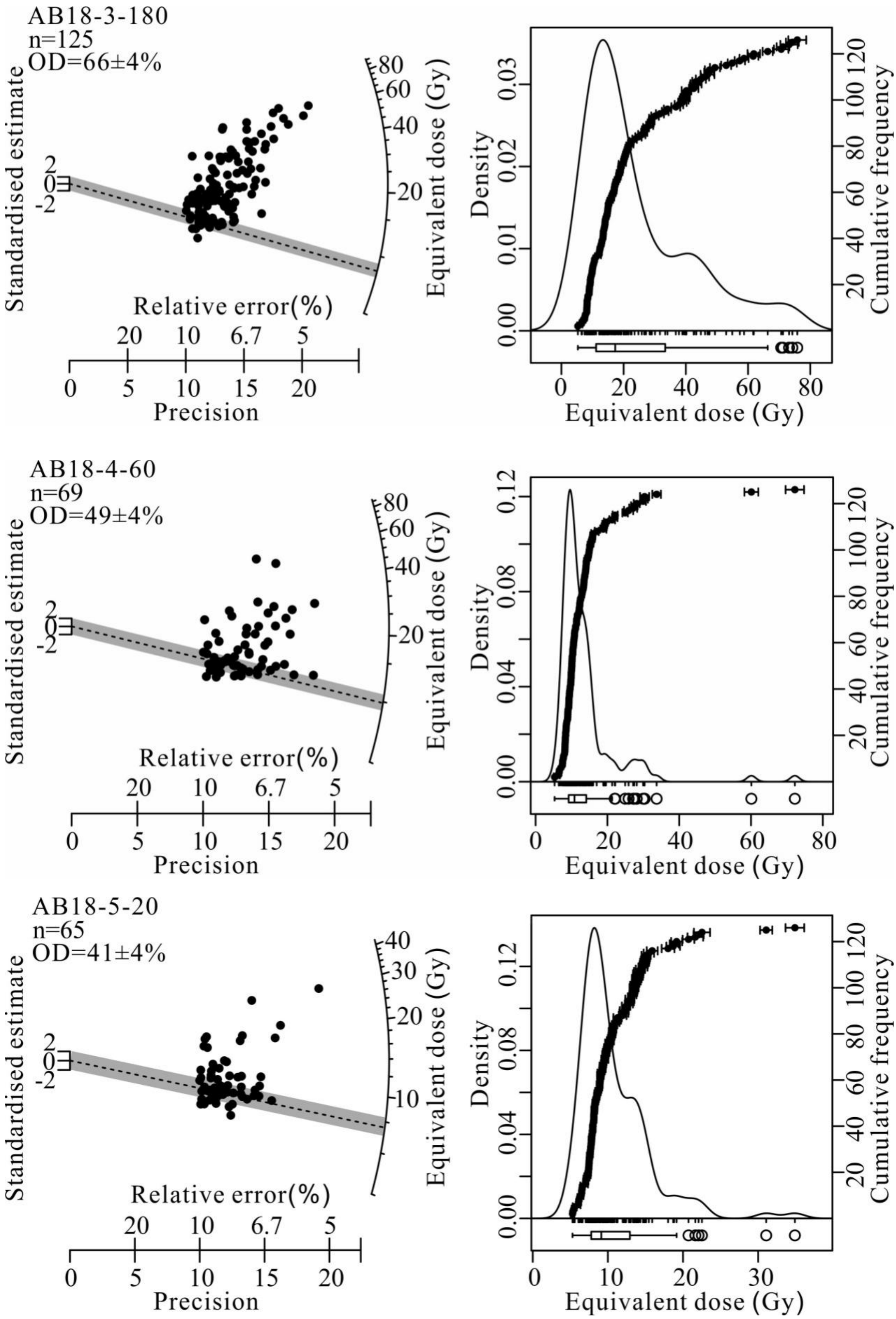
AB18-3-180
n=125
OD=66±4%
Standardised estimate
Relative error(%)
Precision
Equivalent dose (Gy)
Density
Cumulative frequency
AB18-4-60
n=69
OD=49±4%
Standardised estimate
Relative error(%)
Precision
Equivalent dose (Gy)
Density
Cumulative frequency
AB18-5-20
n=65
OD=41±4%
Standardised estimate
Relative error(%)
Precision
Equivalent dose (Gy)
Density
Cumulative frequency

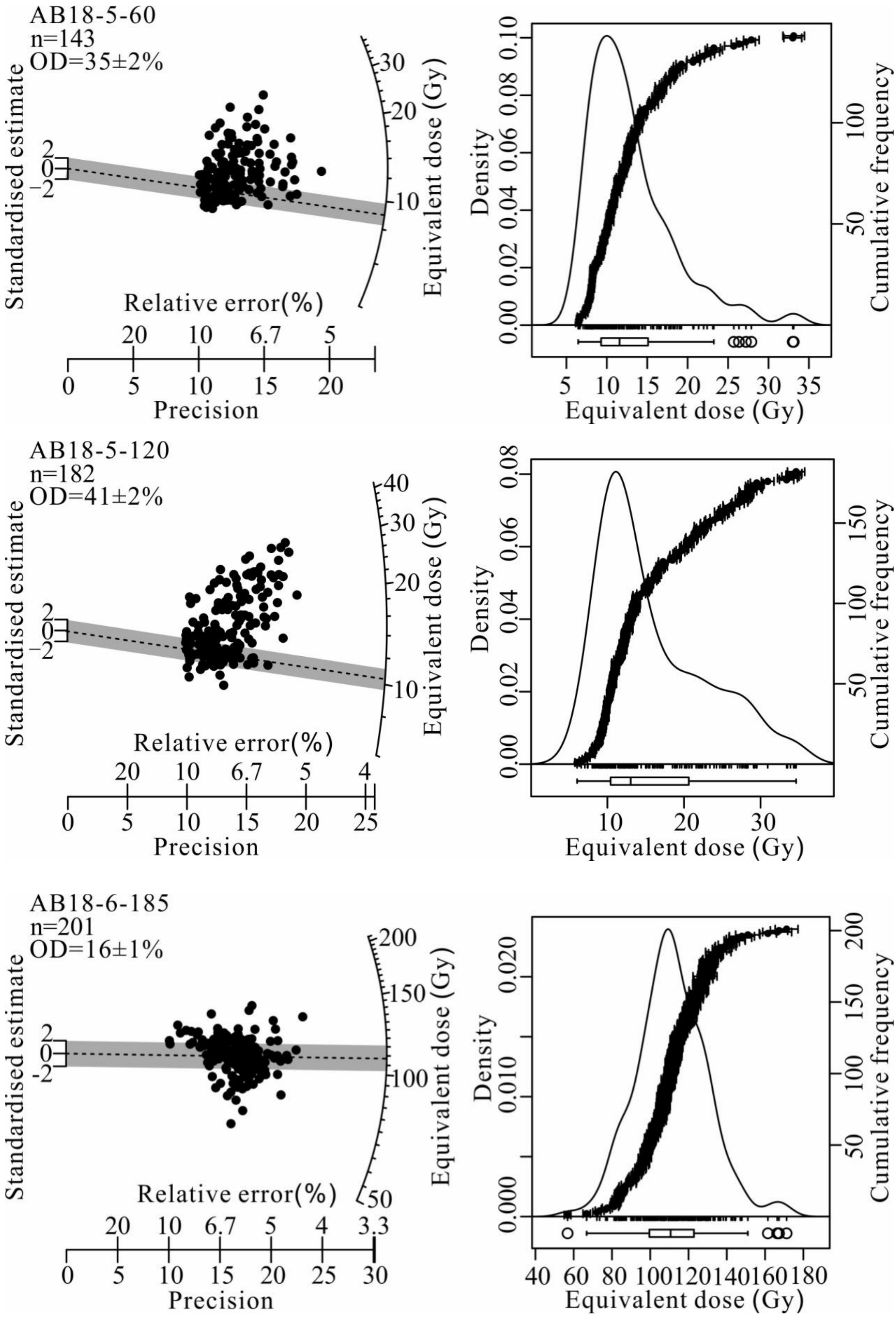
AB18-5-60
n=143
OD=35±2%
Standardised estimate
Relative error(%)
Precision
Equivalent dose (Gy)
Density
Cumulative frequency
AB18-5-120
n=182
OD=41±2%
AB18-6-185
n=201
OD=16±1%

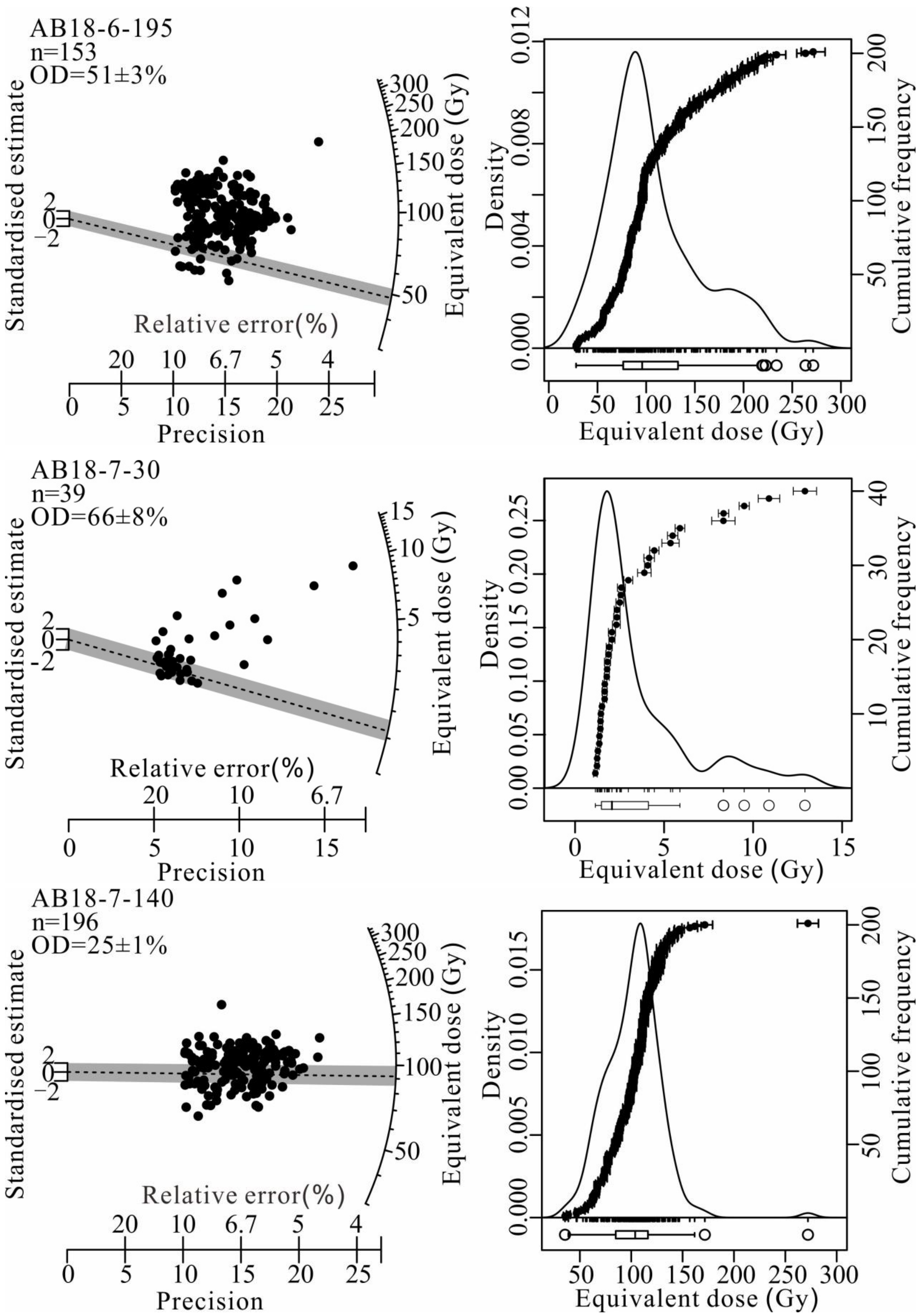
AB18-6-195
n=153
OD=51±3%
Standardised estimate
Relative error(%)
Precision
Equivalent dose (Gy)
Density
Cumulative frequency
AB18-7-30
n=39
OD=66±8%
Standardised estimate
Relative error(%)
Precision
Equivalent dose (Gy)
Density
Cumulative frequency
AB18-7-140
n=196
OD=25±1%
Standardised estimate
Relative error(%)
Precision
Equivalent dose (Gy)
Density
Cumulative frequency

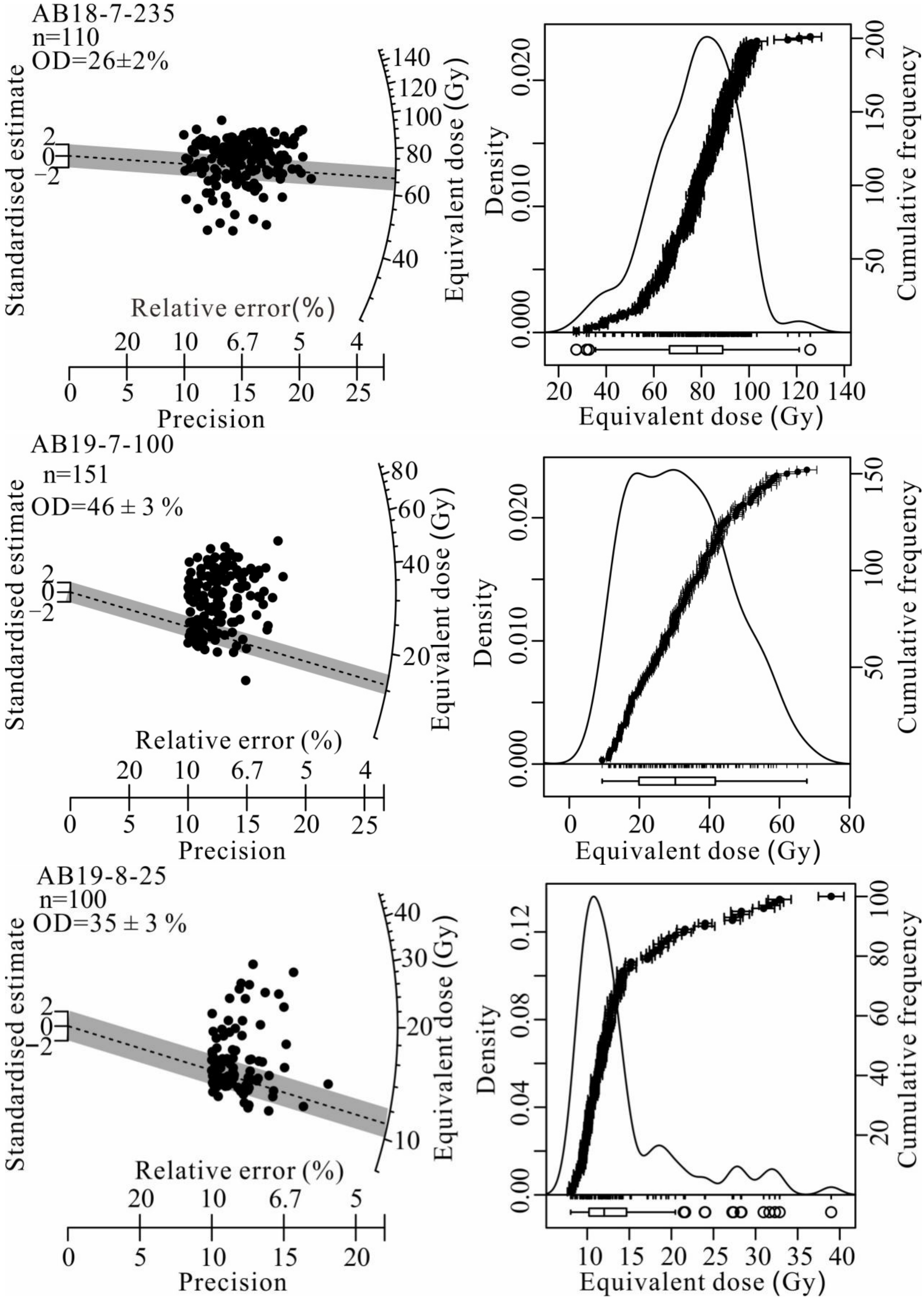
AB18-7-235
n=110
OD=26±2%
Standardised estimate
Relative error(%)
Precision
Equivalent dose (Gy)
Density
Cumulative frequency
AB19-7-100
n=151
OD=46 ± 3 %
Standardised estimate
Relative error (%)
Precision
Equivalent dose (Gy)
Density
Cumulative frequency
AB19-8-25
n=100
OD=35 ± 3 %
Standardised estimate
Relative error (%)
Precision
Equivalent dose (Gy)
Density
Cumulative frequency

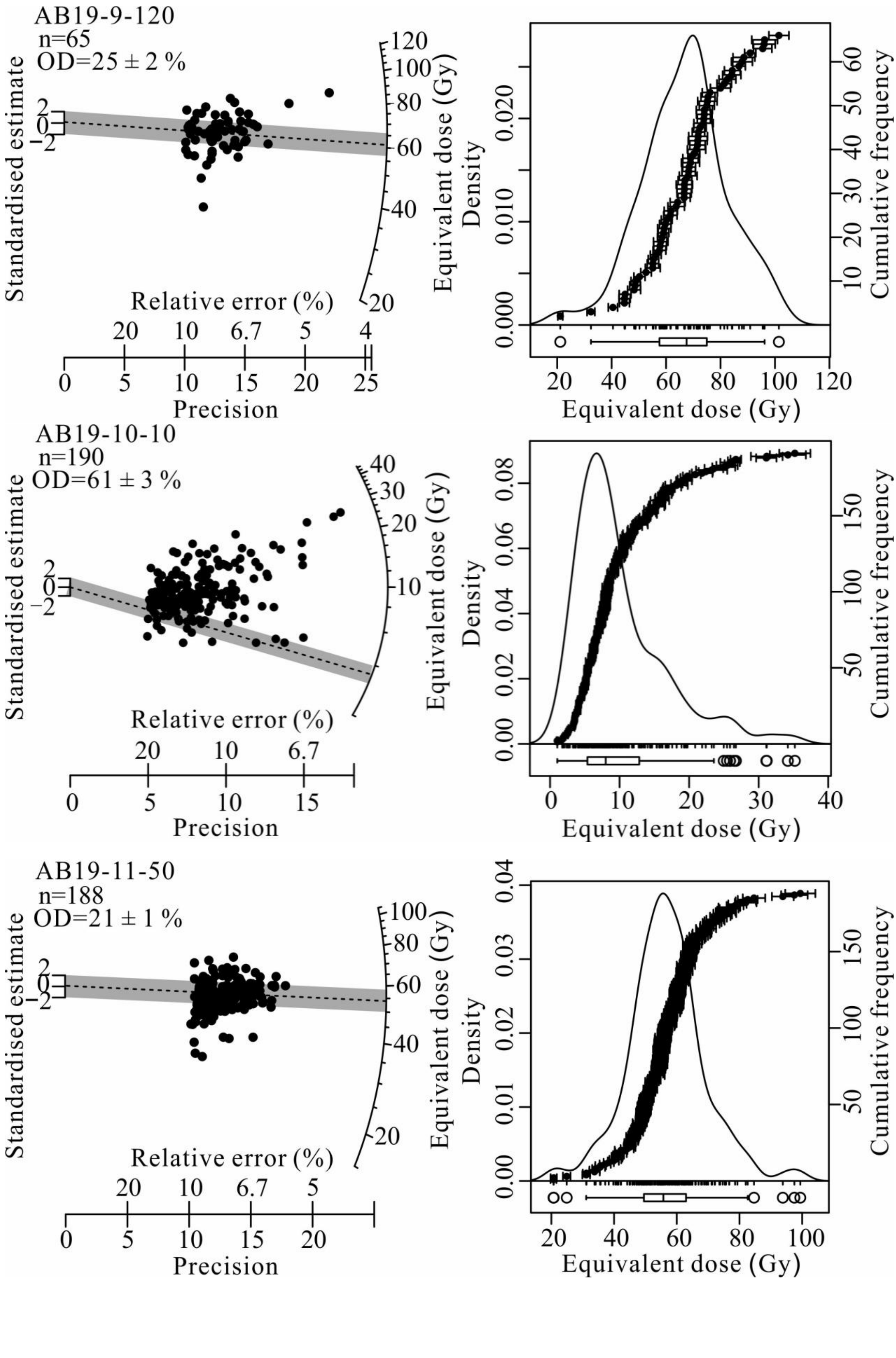
AB19-9-120
n=65
OD=25 ± 2 %
Standardised estimate
Equivalent dose (Gy)
Relative error (%)
Precision
Density
Cumulative frequency
Equivalent dose (Gy)
AB19-10-10
n=190
OD=61 ± 3 %
Standardised estimate
Equivalent dose (Gy)
Relative error (%)
Precision
Density
Cumulative frequency
Equivalent dose (Gy)
AB19-11-50
n=188
OD=21 ± 1 %
Standardised estimate
Equivalent dose (Gy)
Relative error (%)
Precision
Density
Cumulative frequency
Equivalent dose (Gy)

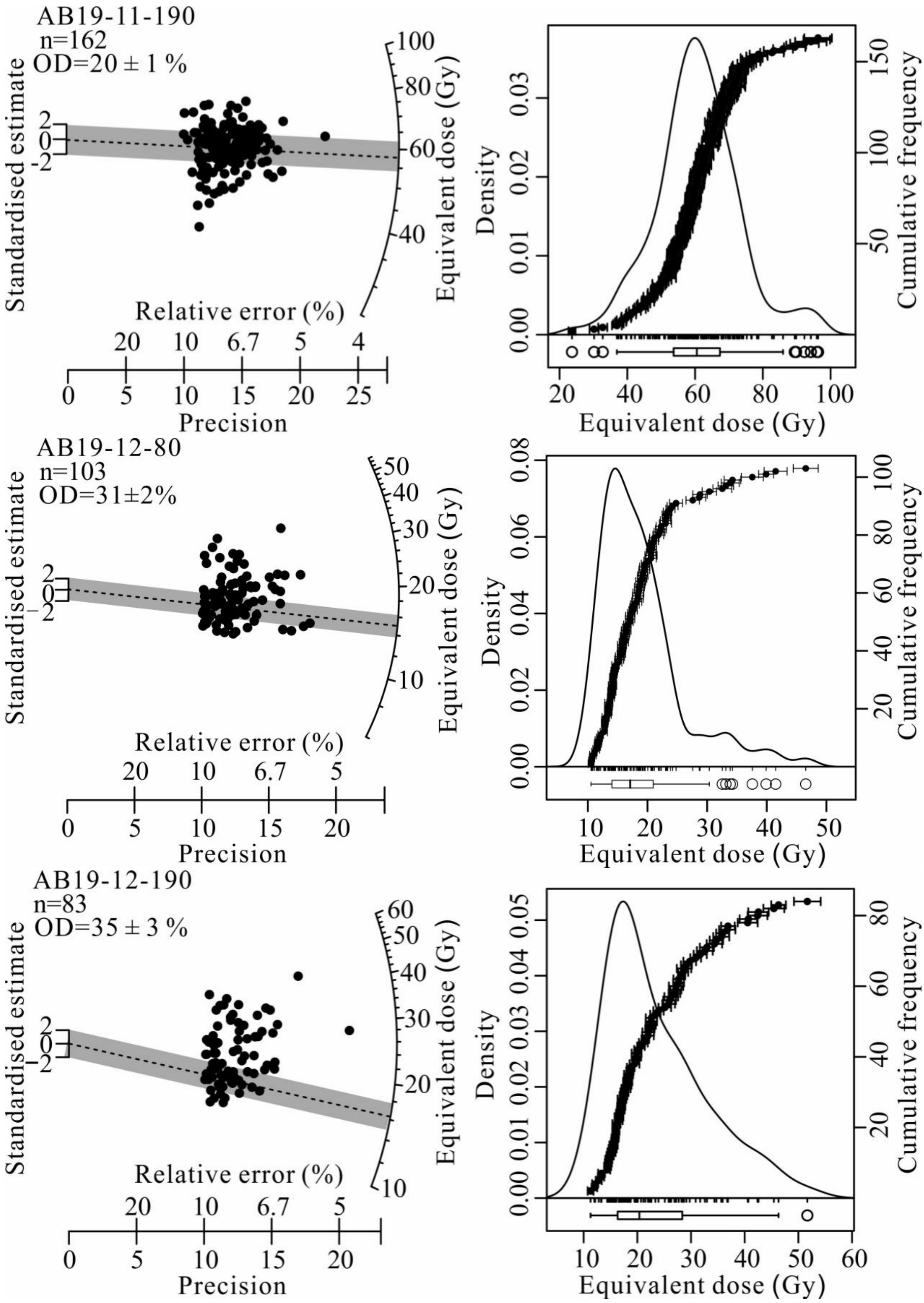

AB19-11-190
n=162
OD=20 ± 1 %
Standardised estimate
Relative error (%)
Precision
Equivalent dose (Gy)
Density
Cumulative frequency
AB19-12-80
n=103
OD=31±2%
AB19-12-190
n=83
OD=35 ± 3 %

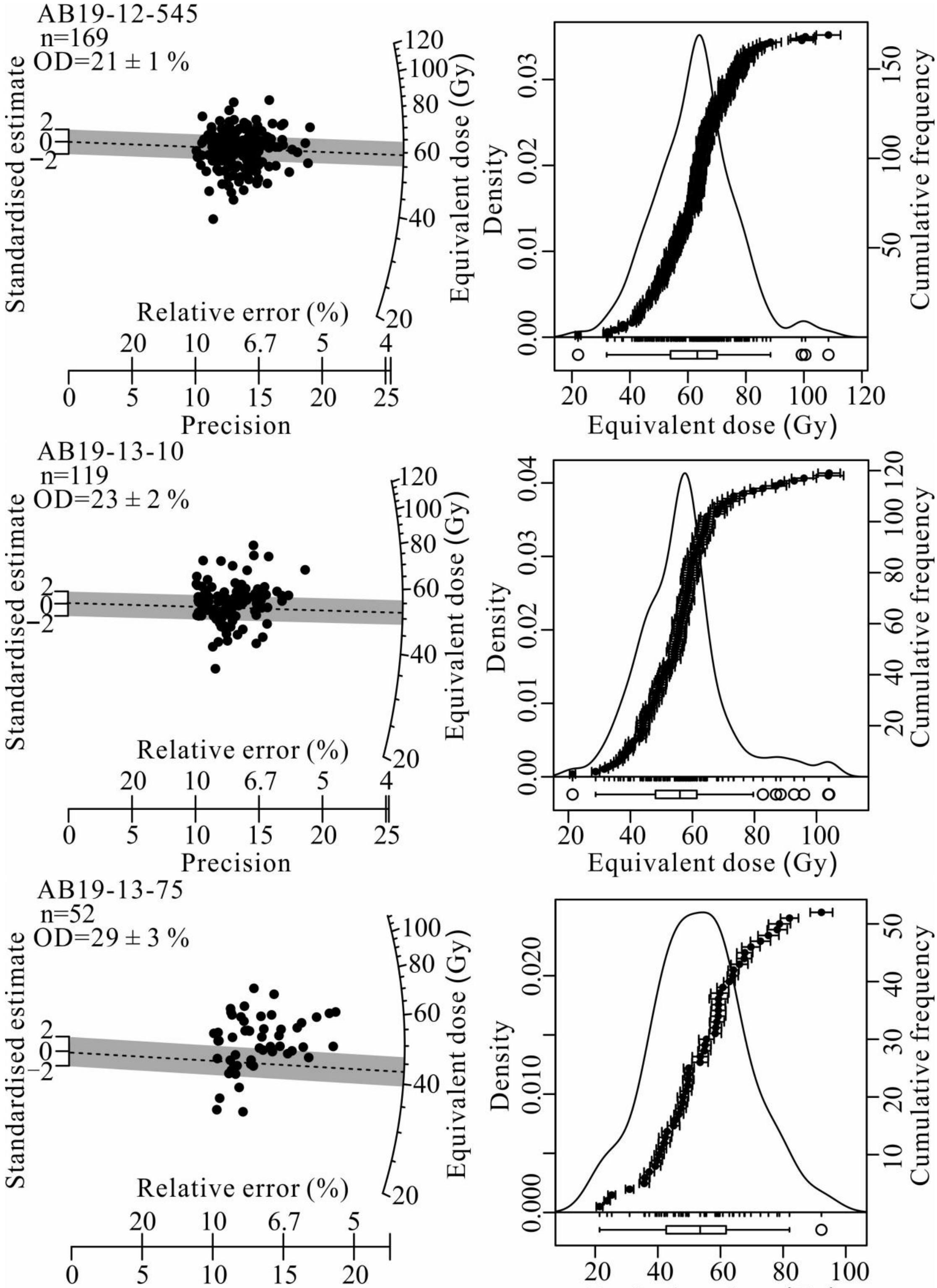
AB19-12-545
n=169
OD=21 ± 1 %
AB19-13-10
n=119
OD=23 ± 2 %
AB19-13-75
n=52
OD=29 ± 3 %
Standardised estimate
Relative error (%)
Precision
Equivalent dose (Gy)
Density
Cumulative frequency

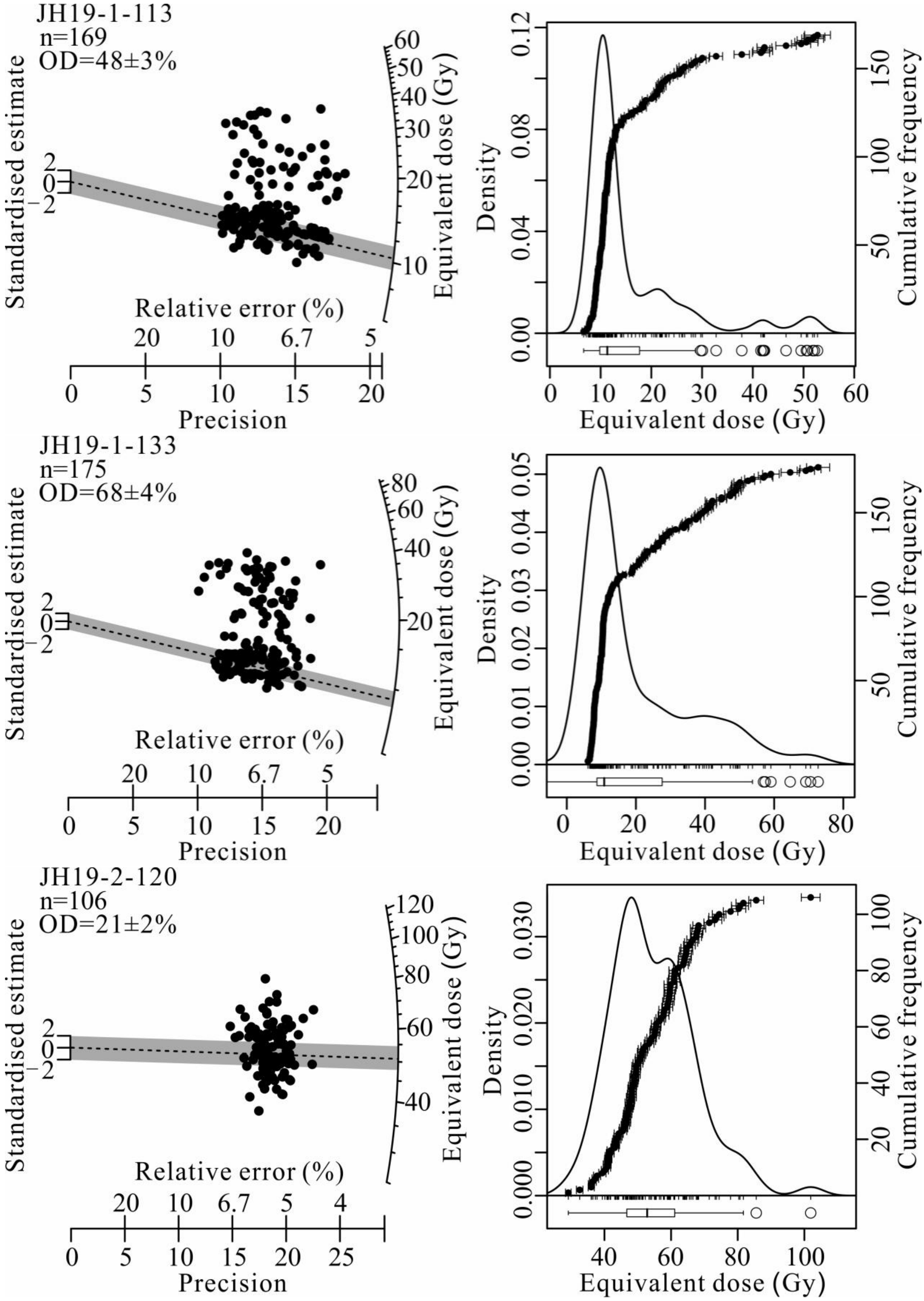
JH19-1-113
n=169
OD=48±3%
Standardised estimate
Relative error (%)
Precision
Equivalent dose (Gy)
Density
Cumulative frequency
JH19-1-133
n=175
OD=68±4%
JH19-2-120
n=106
OD=21±2%

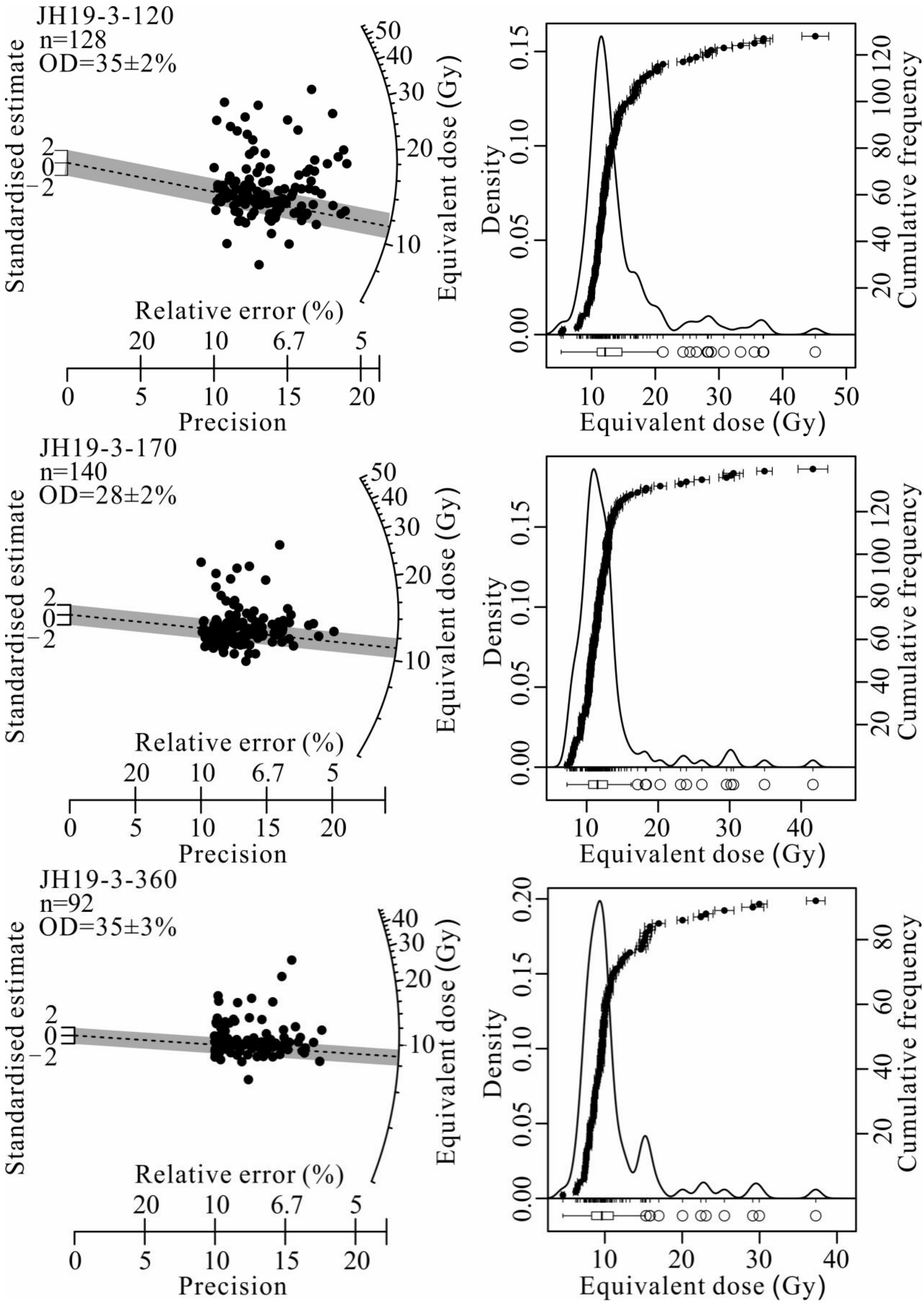
JH19-3-120
n=128
OD=35±2%
Standardised estimate
Relative error (%)
Precision
Equivalent dose (Gy)
Density
Cumulative frequency
JH19-3-170
n=140
OD=28±2%
JH19-3-360
n=92
OD=35±3%

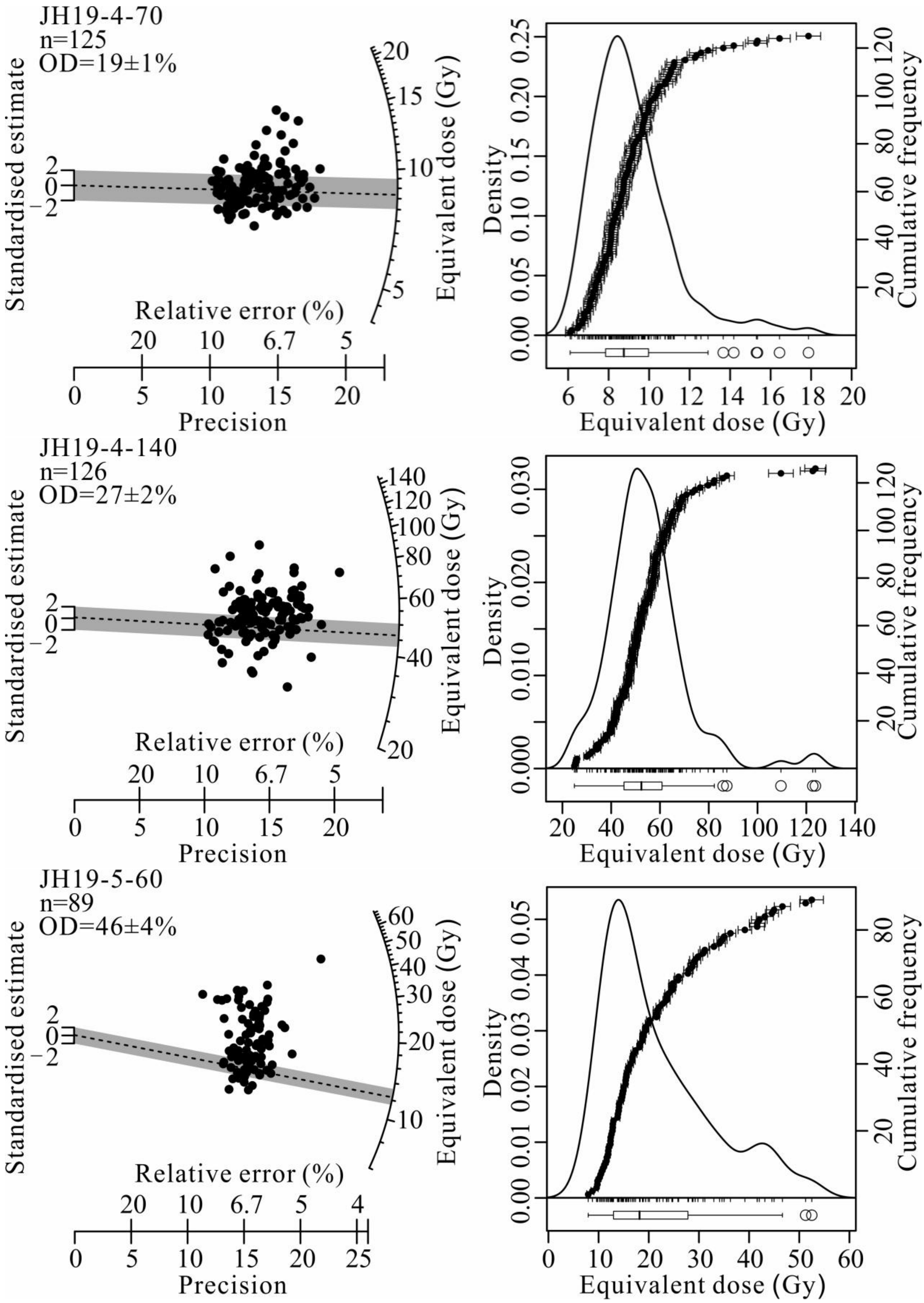
JH19-4-70
n=125
OD=19±1%
Standardised estimate
Equivalent dose (Gy)
Relative error (%)
Precision
Density
Cumulative frequency
Equivalent dose (Gy)
JH19-4-140
n=126
OD=27±2%
JH19-5-60
n=89
OD=46±4%

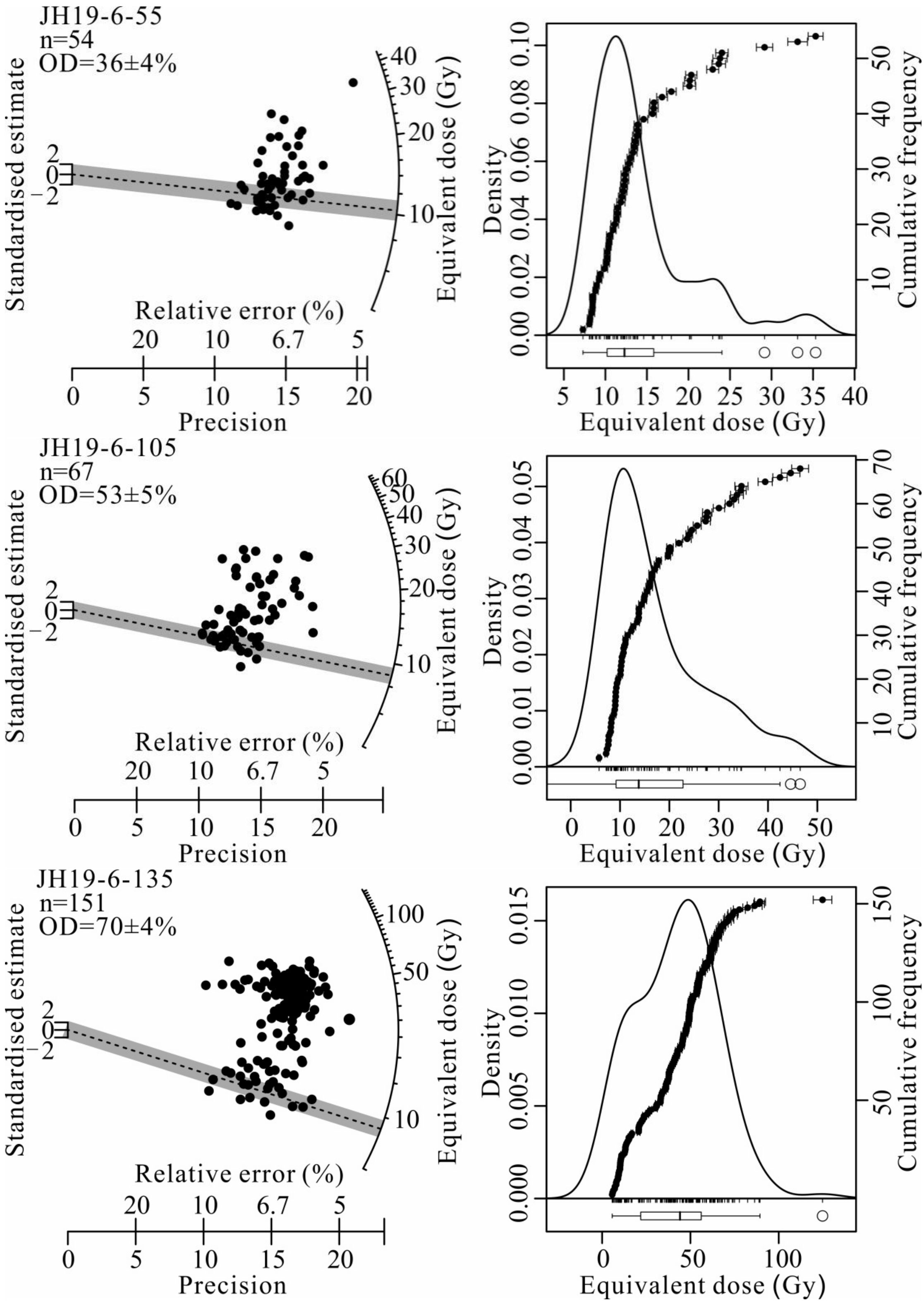

Figure S4. Abanico plots (left) and Kernel Density Estimates (KDEs; right) of all single-grain samples from the shorelines in the Aibi Lake Basin.

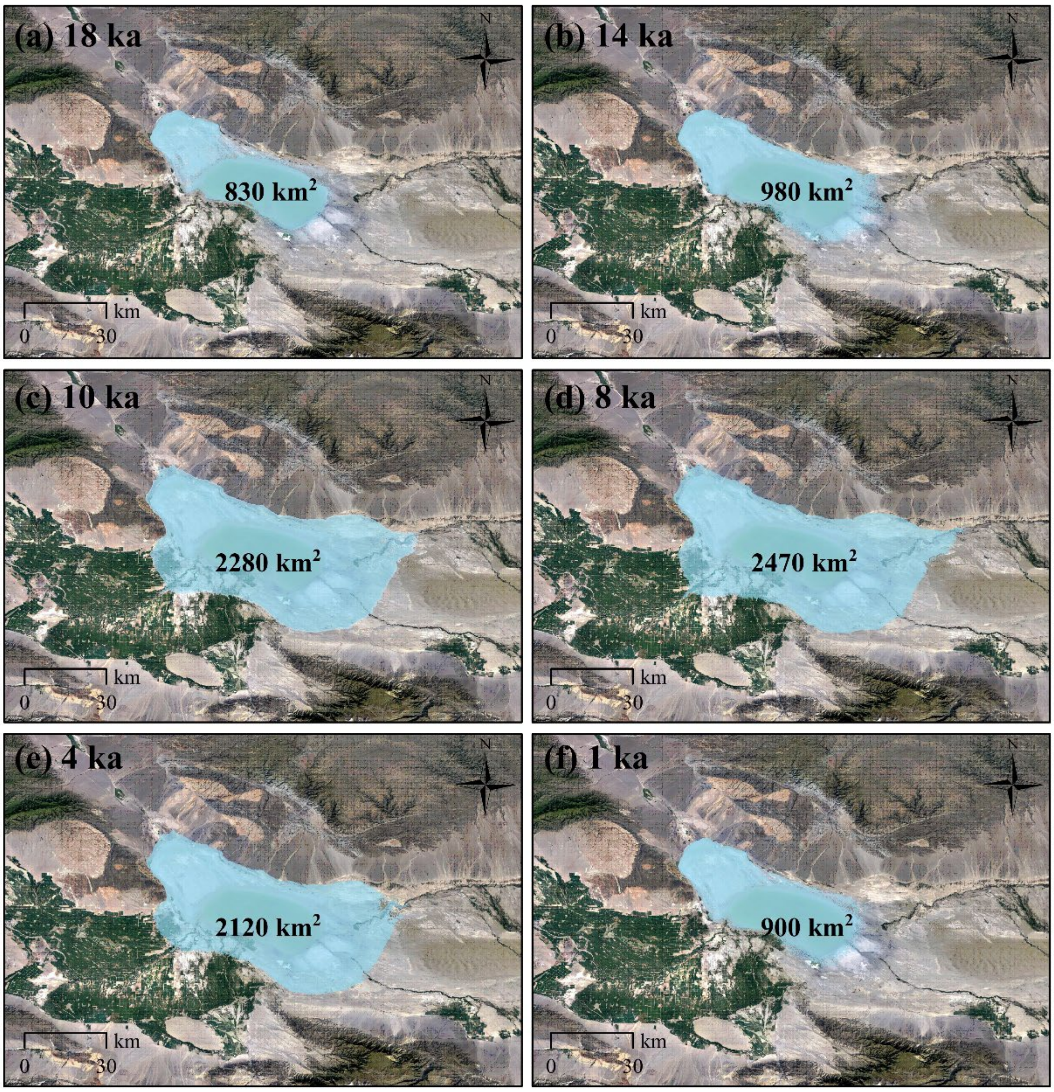

Figure S5. The reconstructed lake covering area changes of Aibi Lake during past 18 ka.

Table S1. Information for samples collected from paleoshorelines in the Aibi Lake Basin.

Section	Elevation (m)	Longitude	Latitude	Above modern lake level (m)
AB18-1	229	82°37'33.33"	45°09'21.49"	35
AB18-2	225	82°37'35.18"	45°09'17.73"	31
AB18-3	223	82°38'15.96"	45°09'19.83"	29
AB18-4	219	82°38'25.55"	45°09'07.16"	25
AB18-5	209	82°39'19.35"	45°08'42.11"	15
AB18-6	203	82°39'00.10"	45°08'18.06"	9
AB18-7	198	82°38'51.34"	45°07'56.37"	4
AB19-7	214	82°34'39.977"	45°04'10.601"	20
AB19-8	208	82°34'48.945"	45°03'56.949"	14
AB19-9	200	82°35'15.328"	45°04'10.601"	6
AB19-10	197	82°35'18.135"	45°04'03.580"	3
AB19-11	226	82°34'14.704"	45°04'12.810"	32
AB19-12	221	82°34'17.447"	45°04'03.550"	27
AB19-13	230	82°34'49.330"	45°05'06.117"	36
JH19-1	205	83°03'12.023"	44°41'12.217"	11
JH19-2	224	83°14'01.662"	44°37'50.373"	30
JH19-3	221	83°13'51.265"	44°38'00.234"	27
JH19-4	208	83°10'34.753"	44°39'10.176"	14
JH19-5	201	83°02'44.225"	44°41'28.306"	7
JH19-6	203	83°02'44.694"	44°41'25.487"	9

Table S2. Protocol for quartz OSL dating and K-feldspar single-aliquot and single-grain pIRIR dating used for the D_e measurements of shoreline samples.

Step	Quartz SAR dating protocol	Observed	Single-aliquot $pIR_{50}IR_{170}$ dating protocol	Observed	Single-grain $pIR_{50}IR_{170}$ dating protocol	Observed
1	Give dose D_i		Give dose D_i		Give dose D_i	
2	Preheat, 220 ºC, 10 s		Preheat at 200 °C for 60 s		Preheat at 200 °C for 60 s	
3	IRSL, 40 s at 50 ºC		IRSL, 200 s at 50 ºC	L_{X1}	IRSL, (laser, 2 s at 50 ºC)	L_{X1}
4	OSL, 40 s at 125 ºC	L_x	pIRIR, 200 s at 170 ºC	L_{X2}	IRSL, (laser, 2 s at 170ºC)	L_{X2}
5	Give test dose		Give test dose		Give test dose	
6	Preheat, 180 ºC, 10 s		Preheat at 200 °C for 60 s		Preheat at 200 °C for 60 s	
7	IRSL, 40 s at 50 ºC		IRSL, 200 s at 50 ºC	T_{X1}	IRSL, (laser, 2 s at 50 ºC)	T_{X1}
8	OSL, 40 s at 125 ºC	T_x	pIRIR, 200 s at 170 ºC	T_{X2}	IRSL, (laser, 2 s at 170ºC)	T_{X2}
9	Illumination, 40 s at 280 ºC		IRSL, 100 s bleaching at 205 ºC		IRSL, 100 s at 205 ºC	
10	Return to 1		Return to 1		Return to 1	

Table S3. Summary of the residual doses for the IR_{50} and $pIR_{50}IR_{170}$ signals after 28h bleaching under sunlight for the single-aliquot K-feldspar samples from the Aibi Lake Basin shorelines.

Sample No.	IR residual dose (Gy)	pIRIR residual dose (Gy)
AB18-1-65	0.14±0.01	0.35±0.01
AB18-1-180	0.16±0.01	0.38±0.02
AB18-1-190	0.20±0.01	0.56±0.04
AB18-2-70	0.17±0.01	0.36±0.02
AB18-3-45	0.11±0.00	0.27±0.01
AB18-3-170	0.12±0.00	0.17±0.01
AB18-3-180	0.09±0.00	0.27±0.01
AB18-4-60	0.18±0.01	0.21±0.01
AB18-5-20	0.08±0.01	0.13±0.01
AB18-5-60	0.11±0.01	0.19±0.01
AB18-5-120	0.06±0.00	0.13±0.01
AB18-6-185	0.08±0.00	0.22±0.01
AB18-6-195	0.14±0.01	0.27±0.01
AB18-7-30	0.11±0.00	0.15±0.01
AB18-7-140	0.12±0.00	0.20±0.01
AB18-7-235	0.12±0.00	0.18±0.01
AB19-7-100	0.07±0.00	0.30±0.02
AB19-8-25	0.00±0.00	0.16±0.06
AB19-9-120	0.10±0.01	0.52±0.02
AB19-10-10	0.03±0.00	0.28±0.02
AB19-11-50	0.07±0.03	0.36±0.02
AB19-11-190	0.08±0.01	0.53±0.02
AB19-12-80	0.05±0.01	0.27±0.02
AB19-12-190	0.02±0.03	0.14±0.03
AB19-12-545	0.08±0.01	0.45±0.03
AB19-13-10	0.09±0.04	0.49±0.04
AB19-13-75	0.08±0.01	0.40±0.03
JH19-1-113	0.02±0.02	0.11±0.01
JH19-1-133	0.00±0.00	0.17±0.02
JH19-2-120	0.01±0.01	0.31±0.03
JH19-2-205	0.03±0.00	0.22±0.01
JH19-3-120	0.00±0.00	0.09±0.05
JH19-3-170	0.00±0.00	0.04±0.01
JH19-3-360	0.00±0.00	0.03±0.03
JH19-4-70	0.00±0.00	0.00±0.00
JH19-4-100	0.00±0.00	0.00±0.00
JH19-4-140	0.11±0.02	0.25±0.03
JH19-5-60	0.04±0.00	0.26±0.02
JH19-5-100	0.04±0.01	0.48±0.02
JH19-5-200	0.06±0.01	0.42±0.02
JH19-6-55	0.04±0.00	0.27±0.04
JH19-6-105	0.06±0.00	0.31±0.01
JH19-6-135	0.03±0.00	0.31±0.01
JH19-6-170	0.05±0.01	0.41±0.03

Table S4. Summary of the single-aliquot pIRIR ages and the single-grain pIRIR CAM ages for the K-feldspar samples from paleoshorelines in the Aibi Lake Basin.

Sample. No	Altitude (m)	Single-aliquot pIRIR D_e (Gy)	OD of Single aliquot pIRIR D_e (%)	Single-grain pIRIR D_e (Gy)	OD of Single-grain CAM D_e (%)	Single-aliquot pIRIR age (ka)	Single-grain pIRIR CAM age (ka)
AB18-1-65	227.43	63.0±3.0	11±3	48.7±1.2	33±2	15.0±0.9	11.6±0.5
AB18-1-180	228.58	71.6±4.6	22±5	51.1±2.2	40±3	16.3±1.2	11.7±0.7
AB18-1-190	228.68	81.3±5.7	24±5	53.0±2.2	36±3	20.4±1.6	13.3±0.8
AB18-2-70	224.33	73.6±4.3	14±4	48.9±1.6	34±2	19.5±1.4	13.0±0.7
AB18-3-45	222.58	21.8±1.0	11±3	15.4±0.9	48±4	5.3±0.3	3.7±0.3
AB18-3-170	221.33	26.5±2.1	27±6	15.6±0.7	42±3	6.7±0.6	4.0±0.2
AB18-3-180	221.23	24.9±2.4	31±7	19.4±1.2	66±4	5.2±0.5	4.0±0.3
AB18-4-60	218.43	16.2±0.7	9±3	13.4±0.8	49±4	4.0±0.2	3.3±0.2
AB18-5-20	208.83	14.1±0.8	14±4	9.6±0.5	41±4	3.6±0.2	2.4±0.2
AB18-5-60	208.43	15.5±0.3	4±2	12.1±0.4	35±2	3.9±0.2	3.0±0.2
AB18-5-120	207.83	16.2±0.9	19±4	14.5±0.4	41±2	4.1±0.3	3.7±0.2
AB18-6-185	201.18	118.8±2.3	4±2	109.6±1.3	16±1	28.2±1.1	26.0±0.9
AB18-6-195	201.08	145.5±9.3	21±5	100.2±4.1	51±3	36.2±2.7	24.9±1.4
AB18-7-30	197.73	3.6±0.4	42±8	2.7±0.3	66±8	0.9±0.1	0.7±0.1
AB18-7-140	196.63	103.4±1.7	3±1	99.5±1.9	25±1	28.6±1.5	27.5±1.5
AB18-7-235	195.68	89.8±3.4	9±3	72.5±1.8	26±2	24.8±1.6	20.0±1.2
AB19-7-100	213.00	24.9±1.1	15±3	28.9±1.1	46±3	4.7±0.3	5.5±0.3
AB19-8-25	207.75	11.0±0.4	11±2	13.2±0.5	35±3	2.4±0.1	2.8±0.1
AB19-9-120	198.80	60.2±0.8	2±1	65.0±2.1	25±2	13.7±0.6	14.8±0.7
AB19-10-10	196.90	4.8±0.4	28±6	8.3±0.4	61±3	1.0±0.1	1.7±0.1
AB19-11-50	225.50	50.3±0.9	6±1	55.4±0.9	21±1	13.3±0.6	14.7±0.7
AB19-11-190	224.10	51.5±1.2	6±2	59.4±1.0	20±1	10.5±0.5	12.1±0.5
AB19-12-80	220.20	16.3±0.5	8±2	16.3±0.5	31±2	3.5±0.2	3.5±0.2
AB19-12-190	219.10	19.5±0.4	7±1	22.0±0.9	35±3	4.1±0.2	4.6±0.3
AB19-12-545	215.55	56.1±0.8	4±1	60.8±1.1	21±1	11.6±0.5	12.5±0.5
AB19-13-10	229.90	54.0±1.4	6±2	54.7±1.2	23±2	10.2±0.5	10.3±0.5
AB19-13-75	229.25	49.5±1.7	12±2	51.2±2.1	29±3	9.5±0.5	9.8±0.5
JH19-1-113	203.87	19.7±1.6	30±6	13.5±0.5	48±3	4.2±0.4	2.9±0.2
JH19-1-133	203.67	19.0±1.4	26±5	15.3±0.8	68±4	4.2±0.3	3.4±0.2
JH19-2-120	222.80	53.5±1.0	4±1	53.4±1.1	21±2	12.4±0.5	12.3±0.5
JH19-2-205	221.95	46.1±0.8	4±1	48.2±0.7	17±1	10.9±0.5	11.4±0.5
JH19-3-120	219.80	13.2±1.0	26±5	13.3±0.4	35±2	2.9±0.2	3.0±0.1
JH19-3-170	219.30	12.7±0.4	12±2	11.9±0.3	28±2	2.9±0.1	2.7±0.1
JH19-3-360	217.40	10.9±0.6	18±4	10.3±0.4	35±3	2.7±0.2	2.6±0.1
JH19-4-70	207.30	9.7±0.3	11±2	9.0±0.2	19±1	2.4±0.1	2.2±0.1
JH19-4-100	207.00	9.4±0.3	11±2	9.8±0.2	15±1	2.3±0.1	2.4±0.1
JH19-4-140	206.60	46.1±2.1	16±3	52.3±1.3	27±2	11.9±0.7	13.5±0.6
JH19-5-60	200.40	24.2±1.0	14±3	19.2±1.0	46±4	5.3±0.3	4.2±0.3
JH19-5-100	200.00	59.5±0.7	2±1	61.1±1.2	24±1	13.6±0.5	13.9±0.6

JH19-5-200	199.00	53.5±0.8	3±1	59.0±1.1	23±1	12.7±0.5	14.0±0.6
JH19-6-55	202.45	18.0±0.7	13±3	13.1±0.7	36±4	4.0±0.2	2.9±0.2
JH19-6-105	201.95	17.6±0.7	12±3	14.9±1.0	53±5	4.0±0.2	3.4±0.3
JH19-6-135	201.65	41.7±1.2	8±2	34.2±2.0	70±4	9.7±0.4	8.0±0.5
JH19-6-170	201.30	55.8±1.6	9±2	60.9±0.9	19±1	14.0±0.6	15.3±0.6

Table S5. Summary of accepted grains passing the rejection criteria for K-feldspar samples from the Aibi Lake Basin.

Sample No.	Measured grains	Brightest 30% grains*	Rejection criteria (see footnotes)								Rejected grains	Accepted grains
			1	2	3	4	5	6	7	8		
AB18-1-65	800	240	1	0	3	52	0	0	4	0	60	180
AB18-1-180	700	210	2	0	9	107	0	0	2	0	120	90
AB18-1-190	700	210	1	0	19	96	0	0	15	0	131	79
AB18-2-70	700	210	2	0	5	88	0	0	4	0	99	111
AB18-3-45	700	210	3	0	116	12	0	1	3	0	135	75
AB18-3-170	700	210	6	1	86	12	0	0	5	0	110	100
AB18-3-180	900	270	5	0	71	65	0	0	4	0	145	125
AB18-4-60	700	210	13	4	107	12	0	0	5	0	141	69
AB18-5-20	700	210	11	2	107	18	0	0	7	0	145	65
AB18-5-60	700	210	1	0	50	8	0	0	8	0	67	143
AB18-5-120	700	210	0	0	21	4	0	0	3	0	28	182
AB18-6-185	700	210	1	0	6	2	0	0	0	0	9	201
AB18-6-195	700	210	4	0	41	5	0	0	7	0	57	153
AB18-7-30	800	240	13	5	167	1	0	8	7	0	201	39
AB18-7-140	800	240	7	0	29	7	0	0	1	0	44	196
AB18-7-235	500	150	0	0	25	6	0	1	8	0	40	110
AB19-7-100	800	240	2	0	78	5	0	0	4	0	89	151
AB19-8-25	1400	420	12	0	292	13	0	0	3	0	320	100
AB19-9-120	1300	390	141	96	86	1	0	0	1	0	325	65
AB19-10-10	1100	330	4	0	124	0	0	8	4	0	140	190
AB19-11-50	700	210	2	0	10	10	0	0	0	0	22	188
AB19-11-190	600	180	6	0	7	5	0	0	0	0	18	162
AB19-12-80	1100	330	13	1	210	2	0	0	1	0	227	103
AB19-12-190	700	210	2	0	116	4	0	0	5	0	127	83
AB19-12-545	600	180	1	0	6	4	0	0	0	0	11	169
AB19-13-10	1300	390	64	49	146	10	0	1	1	0	271	119
AB19-13-75	200	60	0	0	7	1	0	0	0	0	8	52

JH19-1-113	800	240	7	0	19	43	0	0	2	0	71	169
JH19-1-133	700	210	5	0	3	25	0	0	2	0	35	175
JH19-2-120	500	150	23	0	4	13	0	0	4	0	44	106
JH19-2-205	600	180	1	0	5	9	0	0	0	0	15	165
JH19-3-120	600	180	3	0	18	31	0	0	0	0	52	128
JH19-3-170	800	240	6	0	9	81	1	1	2	0	100	140
JH19-3-360	1000	300	17	0	2	110	77	0	2	0	208	92
JH19-4-70	800	240	3	0	11	99	0	0	2	0	115	125
JH19-4-100	600	180	2	0	5	52	0	0	0	0	59	121
JH19-4-140	500	150	6	0	9	9	0	0	0	0	24	126
JH19-5-60	400	120	1	0	1	29	0	0	0	0	31	89
JH19-5-100	600	180	3	0	2	10	0	0	0	0	15	165
JH19-5-200	600	180	1	0	0	16	0	0	0	0	17	163
JH19-6-55	400	120	1	0	5	60	0	0	0	0	66	54
JH19-6-105	400	120	2	0	4	46	0	0	1	0	53	67
JH19-6-135	600	180	7	0	3	18	0	0	1	0	29	151
JH19-6-170	800	240	3	0	10	33	0	0	3	0	49	191

Notes: Rejection criteria are as follows: Criteria 1 are recycling ratio limits (15%); criteria 2 is a max test dose error (> 10%); criteria 3 is maximum palaeodose error (> 10%); criteria 4 is maximum recuperation of the largest regeneration dose signal (> 5%); criteria 5 is that the T_n signal > 3σ above background; criteria 6 are any negative D_e values; criteria 7 are any D_e values obtained by extrapolation of the dose-response curve beyond the largest regenerative dose; criteria 8 is if the dose response curve fit is not good.

Table S6. Summary of single-grain pIRIR dating results for samples from the Aibi Lake Basin.

Sample No.	Altitude (m)	Grain size (μm)	Effective grains/All grains	Single grain pIRIR D_e (Gy)	U (ppm)	Th (ppm)	K (%)	Rb (ppm)	W.C. (%)	Cosmic dose rate (Gy/ka)	Dose rate (Gy/ka)	Single-grain pIRIR MAM age (ka)
AB18-1-65	227.43	180-250	180/800	39.0±2.5	1.77±0.3	5.89±0.6	2.37±0.04	65.7±3	5±2.5	0.18±0.02	4.21±0.16	9.3±0.7
AB18-1-180	228.58	180-250	90/700	33.7±2.6	2.20±0.4	6.71±0.6	2.34±0.04	82.7±3	5±2.5	0.23±0.02	4.38±0.18	7.7±0.7
AB18-1-190	228.68	180-250	79/700	39.3±2.9	1.50±0.3	5.00±0.5	2.20±0.04	68.4±3	5±2.5	0.24±0.02	3.99±0.16	9.9±0.8
AB18-2-70	224.33	180-250	111/700	39.0±3.1	1.96±0.3	4.85±0.5	2.05±0.04	68.4±3	10±2.5	0.21±0.02	3.77±0.15	10.3±0.9
AB18-3-45	222.58	180-250	75/700	9.3±0.7	2.16±0.4	6.64±0.6	2.28±0.04	84.6±3	10±2.5	0.23±0.02	4.14±0.17	2.3±0.2
AB18-3-170	221.33	180-250	100/700	10.1±0.8	1.86±0.3	5.85±0.5	2.22±0.04	70.6±3	10±2.5	0.18±0.02	3.93±0.16	2.6±0.2
AB18-3-180	221.23	180-250	125/900	8.7±0.6	6.53±0.5	8.38±0.6	1.92±0.04	75.0±3	10±2.5	0.17±0.02	4.80±0.19	1.8±0.2
AB18-4-60	218.43	180-250	69/700	9.9±0.5	2.09±0.4	5.78±0.5	2.08±0.04	64.8±3	5±2.5	0.21±0.02	4.04±0.17	2.5±0.2
AB18-5-20	208.83	180-250	65/700	7.9±0.4	1.54±0.3	4.71±0.5	2.21±0.04	72.9±3	5±2.5	0.25±0.03	3.95±0.16	2.0±0.1
AB18-5-60	208.43	180-250	143/700	9.2±0.6	1.61±0.3	5.45±0.6	2.2±0.04	76.2±3	5±2.5	0.21±0.02	4.02±0.16	2.3±0.2
AB18-5-120	207.83	180-250	182/700	10.2±0.6	1.50±0.3	5.00±0.5	2.2±0.04	56.0±3	5±2.5	0.17±0.02	3.92±0.16	2.6±0.2
AB18-6-185	201.18	125-150	201/700	108.9±2.1	2.84±0.4	14.73±0.7	2.19±0.04	99.1±3	15±2.5	0.18±0.02	4.21±0.14	25.8±1
AB18-6-195	201.08	180-250	153/700	49.7±4.2	1.94±0.3	7.00±0.6	2.07±0.04	79.2±3	15±5	0.17±0.02	4.02±0.16	12.4±1.2
AB18-7-30	197.73	180-250	39/800	1.6±0.2	1.54±0.3	4.92±0.5	2.15±0.04	66.9±3	5±2.5	0.23±0.02	3.93±0.16	0.42±0.04
AB18-7-140	196.63	180-250	196/800	90.8±6.1	1.98±0.3	6.56±0.6	1.92±0.04	69.4±3	15±5	0.19±0.02	3.62±0.18	25.1±2.2
AB18-7-235	195.68	180-250	110/500	66.1±4.2	2.15±0.4	7.31±0.6	1.98±0.04	79.2±3	15±2.5	0.17±0.02	3.62±0.19	18.3±1.5
AB19-7-100	213.00	180-250	151/800	15.9±1.2	2.57±0.4	11.24±0.7	2.94±0.04	135.5±4	5±2.5	0.19±0.02	5.28±0.20	3.0±0.3
AB19-8-25	207.75	180-250	100/1400	11.2±0.4	1.63±0.3	7.04±0.6	2.76±0.04	119.4±4	5±2.5	0.24±0.02	4.65±0.17	2.4±0.1
AB19-9-120	198.80	180-250	65/1300	61.4±4.1	2.35±0.4	8.86±0.6	2.41±0.04	111.6±4	10±2.5	0.19±0.02	4.40±0.17	14.0±1.1

AB19-10-10	196.90	180-250	190/1100	3.7±0.3	1.81±0.4	8.40±0.6	2.89±0.04	126.4±4	5±2.5	0.27±0.03	4.80±0.19	0.8±0.1
AB19-11-50	225.50	180-250	188/700	54.0±1.9	1.47±0.3	5.47±0.6	1.95±0.04	84.9±3	5±2.5	0.22±0.02	3.77±0.16	14.3±0.8
AB19-11-190	224.10	180-250	162/600	58.5±1.8	1.92±0.4	7.36±0.6	2.98±0.04	134.0±4	5±2.5	0.18±0.02	4.90±0.19	11.9±0.6
AB19-12-80	220.20	180-250	103/1100	15.0±1.1	2.16±0.4	8.71±0.6	2.54±0.04	122.4±4	5±2.5	0.19±0.02	4.66±0.18	3.2±0.3
AB19-12-190	219.10	180-250	83/700	16.7±1.1	2.10±0.4	8.19±0.6	2.75±0.04	128.7±4	5±2.5	0.17±0.02	4.78±0.18	3.5±0.3
AB19-12-545	215.55	180-250	169/600	59.1±2.5	2.24±0.4	8.40±0.6	2.83±0.04	135.2±4	5±2.5	0.12±0.01	4.85±0.19	12.2±0.7
AB19-13-10	229.90	180-250	119/1300	52.0±2.6	5.45±0.5	13.12±0.7	2.27±0.04	116.1±4	5±2.5	0.27±0.03	5.29±0.21	9.8±0.7
AB19-13-75	229.25	180-250	52/200	43.5±3.8	2.53±0.4	8.49±0.6	3.06±0.04	114.6±4	5±2.5	0.2±0.02	5.21±0.19	8.4±0.8
JH19-1-113	203.87	180-250	169/800	10.4±0.3	1.3±0.3	5.88±0.6	2.82±0.04	135.2±4	5±2.5	0.19±0.02	4.66±0.18	2.2±0.1
JH19-1-133	203.67	180-250	175/700	9.0±0.3	1.38±0.3	7.26±0.6	2.71±0.04	136.7±4	5±2.5	0.18±0.02	4.54±0.17	2.0±0.1
JH19-2-120	222.80	180-250	106/500	50.2±2.6	1.56±0.3	5.69±0.6	2.55±0.04	114.9±4	5±2.5	0.19±0.02	4.33±0.17	11.6±0.8
JH19-2-205	221.95	180-250	165/600	47.6±1.2	1.78±0.3	5.85±0.6	2.41±0.04	96.9±4	5±2.5	0.17±0.02	4.24±0.17	11.2±0.5
JH19-3-120	219.80	180-250	128/600	11.5±0.5	3.01±0.4	6.29±0.6	2.35±0.04	101.0±4	5±2.5	0.19±0.02	4.50±0.17	2.6±0.1
JH19-3-170	219.30	150-180	140/800	11.2±0.2	2.56±0.4	4.97±0.5	2.70±0.04	120.4±4	5±2.5	0.18±0.02	4.45±0.16	2.5±0.1
JH19-3-360	217.40	180-250	92/1000	9.0±0.4	1.79±0.3	4.75±0.5	2.28±0.04	101.4±4	5±2.5	0.14±0.01	4.02±0.16	2.3±0.1
JH19-4-70	207.30	150-180	125/800	8.8±0.3	1.62±0.3	5.62±0.6	2.44±0.04	98.3±3	5±2.5	0.2±0.02	4.07±0.14	2.2±0.1
JH19-4-100	207.00	150-180	121/600	9.8±0.2	2.46±0.4	6.89±0.6	2.13±0.04	93.1±4	5±2.5	0.19±0.02	4.03±0.15	2.4±0.1
JH19-4-140	206.60	150-180	126/500	45.3±3.5	1.98±0.4	7.92±0.6	2.18±0.04	97.6±4	10±2.5	0.19±0.02	3.87±0.14	11.7±1.0
JH19-5-60	200.40	180-250	89/400	12.1±1	2.14±0.4	9.78±0.6	2.35±0.04	115.4±4	5±2.5	0.21±0.02	4.56±0.18	2.6±0.2
JH19-5-100	200.00	180-250	165/600	57.7±2.7	1.49±0.3	5.84±0.6	2.81±0.04	128.4±4	10±2.5	0.19±0.02	4.39±0.16	13.2±0.8
JH19-5-200	199.00	180-250	163/600	55.1±2.7	1.45±0.3	5.72±0.6	2.64±0.04	126.0±4	10±2.5	0.17±0.02	4.20±0.16	13.1±0.8
JH19-6-55	202.45	180-250	54/400	10.4±0.9	1.41±0.3	5.32±0.6	2.75±0.04	131.8±4	5±2.5	0.21±0.02	4.48±0.17	2.3±0.2
JH19-6-105	201.95	180-250	67/400	8.8±0.8	1.79±0.3	6.50±0.6	2.55±0.04	123.7±4	5±2.5	0.19±0.02	4.43±0.17	2.0±0.2
JH19-6-135	201.65	150-180	151/600	9.3±0.9	1.49±0.3	5.94±0.6	2.69±0.04	133.7±4	5±2.5	0.19±0.02	4.28±0.14	2.2±0.2
JH19-6-170	201.30	150-180	191/800	59.4±2.1	1.72±0.3	6.96±0.6	2.44±0.04	117.4±4	10±2.5	0.18±0.02	3.99±0.14	14.9±0.7